Addis Ababa University
Addis Ababa Institute of Technology
School of Multidisciplinary Engineering
Center of Renewable Energy

Design, Manufacturing, and Performance Evaluation of Building-Integrated Asymmetric Compound Parabolic Concentrator Solar Evacuated Tube Collector with Concentric Tube Heat Exchanger

A Thesis Submitted to the School of Graduate Studies of Addis Ababa University in Partial Fulfillment of the Requirements for the Award of the Degree of Master of Science in Energy Technology

By:
Biniam Tufa Alemu (GSE/5492/12)

Advisor: Dr. Solomon Tesfamariam

October, 2023

CERTIFICATION

I, the undersigned, certify that I read and hear by recommend for the acceptance by Addis Ababa University, Addis Ababa Institute of Technology, Center of Renewable Energy a thesis entitled “Design, Manufacturing, and Performance Evaluation of a Building-Integrated Asymmetric Compound Parabolic Concentrator Solar Evacuated Tube Collector with Concentric Tube Heat Exchanger". This certificate used as a partial fulfillment of the requirement for the degree of Master of Science in Energy Technology.

Signature _____

Date _____

DECLARATION

I, Biniam Tufa, declare that this thesis is the result of my own work and that all source and material used for this thesis have been duly acknowledged. This thesis is submitted in partial fulfillment of the requirement for master's degree in Energy Technology at Addis Ababa University and to be made available at the university's library under the role of the library. I confidently declare that this thesis has not been submitted to any other institutions anywhere for the award of any academic degree, diploma, or certificate.

Candidate

Name: Biniam Tufa

Signature _____

Date _____

Advisor

Name: Dr. Solomon Tesfamariam (PhD)

Signature _____

Date _____

Addis Ababa University
Addis Ababa Institute of Technology
School of Multidisciplinary
Center of Renewable Energy

Design, Manufacturing, and Performance Evaluation of Building-Integrated Asymmetric Compound Parabolic Concentrator Solar Evacuated Tube Collector with Concentric Tube Heat Exchanger

By: Biniam Tufa Alemu

Approved by Board of Examiners

Dr. Solomon Tesfamariam		
Advisor	Signature	Date
Dr. Mesfin Belayneh		
Internal Examiner	Signature	Date
Dr. Misrak Girma		
External Examiner	Signature	Date
Chairman	Signature	Date
Director of post Graduate Program	Signature	Date

ACKNOWLEDGMENT

I would like to thank and praise God for granting me strength and courage to complete my study and in every step of my life.

First, I would like to express my deepest and heartfelt gratitude to my advisor Dr. Solomon Tesfamariam (PhD) for his continues guidance, suggestion and critical comment. Without his support and motivation this thesis would not have done. Second, my special gratitude goes to Mr. Fitsum Salehu (PhD candidate) for providing me materials and also for his fruitful comments and suggestions. His support was invaluable. I also like to express my gratitude to Dr. Kamil Adem (PhD) for his advice and insightful comment.

My heartfelt gratitude also goes to all members of the Addis Ababa Institute of Technology's Mechanical Engineering Workshop staffs who assisted me in building the prototype. I sincerely appreciate Mr. Israel, Mr. Maseresha, and Mr. Kassaye's invaluable support. I would also want to thank Basil, Anteneh, and other AAiT undergraduate students who helped me during the experiment. Next, I want to express my gratitude to my friends for all of their support during this journey.

Last but not least, I want to convey my sincere gratitude and appreciation to my wife and my family for their unwavering support, love, and kindness.

ABSTRACT

The amount of thermal energy consumed in buildings has increased due to the rapid development of urbanization. In most cases, high-rise buildings have a small ratio of available roof area to the required solar collector area to generate thermal energy. A wall-mounted Asymmetric Compound Parabolic Concentrator (A-CPC) solar evacuated glass tube collector with a concentric tube heat exchanger is designed to boost the solar energy collection for building thermal energy supply. The geometric profile of A-CPC was computed from the standard CPC geometry using solar altitude angles. TracePro and ray-tracing program, were used to predict the collector's optical efficiency. The collector's performance was evaluated using an experimental method in real-world conditions. The optical simulation result shows that, within the range of the solar altitude angle, the highest optical efficiency was around 73% and the average optical efficiency was around 58%. From the experimental result, the average instantaneous thermal efficiency for experiment-1, experiment-2, and experiment-3 was 51.2%, 52.86%, and 53.03%, respectively. Taking systematic and random error into account, the maximum uncertainty of instantaneous thermal efficiency was found to be 6.0%, 5.95%, and 5.94% for experiments 1, 2, and 3, respectively. The findings of this study shows that the A-CPC based collector performance is superior (by 1.63%) and has a high efficiency in comparison to other research studies being conducted in the field. Furthermore, the outcomes shows that, contrary to popular perception, solar collector integration on building walls at low latitude countries is viable and should be taken into consideration.

Keywords: Building-Integrated, Compound Parabolic Concentrator, Ray-tracing, A-CPC, Thermal efficiency

NOMENCLATURE

A_{ap}	Aperture area (m^2)
A_r	Receiver area (m^2)
A_a	Absorber area (m^2)
D	Diameter (mm)
r	Radius of the receiver (mm)
I	Solar irradiation (W/m^2)
L_{CPC}	Length of the collector
Q_u	Useful heat gain (Watts)
Q_s	Solar radiation absorption (Watts)
T_1	Inlet temperature (^oC)
T_2	Outlet temperature (^oC)
ΔT	Change in temperature (^oC)
C	Geometric Concentration ratio
n	i^{th} day of the year
$\dot{m}$	Mass flow rate of the working fluid (kg/s)
v	Volumetric flow rate of the working fluid (m^3/s)
C_p	Specific heat (J/kgK)
ρ	Density of the working fluid (kg/m^3)
$\overline{TT}$	Width of the aperture (mm)
p	Gap loss coefficient
f_{ref}	Multiple reflection coefficients

GREEK SYMBOLS

θ_a	Half-acceptance angle (degree)
α_s	Solar altitude angle (degree)
Φ	Latitude (degree)
δ	Declination angle (degree)
ω	Hour angel (degree)
η_{th}	Thermal efficiency (%)
η_o	Optical efficiency (%)
τ_e	Transmittance of the evacuated glass tube

τ_e	is the dirt stratification factor of the glass envelop
P	Reflectance of the reflective Mylar

ABBREVIATION

2D	Two dimension
3D	Three dimension
A-CPC	Asymmetric Compound Parabolic Concentrator
CPC	Compound Parabolic Concentrator
ES	Ethiopian Standard
ETSC	Evacuated Tube Solar Collector
FPC	Flat Plate Collector
GWh	Gigawatts hour
HVAC	Heating, Ventilation, and Air Conditioning
IEA	International Energy Agency
IRENA	International Renewable Energy Agency
ISO	International Standard Organization
kWh	Kilowatts hour
LiDAR	Light Detection and Ranging
MW	Megawatts
PEA	Petroleum and Energy Authority
PV	Photovoltaic
SWH	Solar Water Heater
EJ	Exajoules

Table of Contents

LIST OF FIGURES

LIST OF TABLES

CHAPTER ONE
INTRODUCTION

1.1. Background

The need for energy is increasing as the globe's population and economic activity increases. Buildings, both residential and commercial ones, are the largest energy consumers. Domestic hot water demand and HVAC (Heating, Ventilation, and Air Conditioning) demand account for the majority of a building's energy consumption. In 2021, the amount of thermal energy consumed in commercial buildings in Addis Ababa was estimated to be 18.7 GWh/year (PEA, 2021). These estimates are expected to increase as a result of growing urbanization and a desire for improved living standards (He *et al.*, 2015). Most of these final energy consumptions are fulfilled by conventional energy sources.

The adoption of solar thermal technologies must be taken into consideration in order to reduce the percentage of conventional thermal energy sources in the building sector. Rooftops of buildings are commonly used to install solar thermal collectors, such as solar water heaters. High-rise buildings, however, have relatively small roof areas and cannot meet the building's thermal energy demand. In contrast, they have large vertical walls that could make them an excellent candidate for collector installation. If all of a building's vertical space is allocated to solar collectors and shading from nearby buildings is neglected, the total annual energy output would triple that of the roof. This percentage will obviously increase as buildings get taller (Brito *et al.*, 2017).

In high-latitude countries, building integration has received much attention. However, low-latitude countries also have the potential to deploy building-integrated systems on vertical surfaces. In contrast to high latitude countries, low latitude countries have high incidence angles but more annual energy is available on vertical surfaces. (Cronemberger, Caamaño-Martín and Sánchez, 2012) revealed that in low-latitude countries, the availability of solar radiation on vertical surfaces is nearly 60%. This demonstrates that, contrary to popular perception, the integration of solar collectors on vertical surfaces at low latitudes is viable and should be considered.

Many research have been done on building-integrated solar collectors. (Lee *et al.*, 2014) developed a wall mounted flat plate collector. The thermal efficiencies was about 22.8%. (Li, Dai and Wang, 2015) developed a balcony mounted U-shaped evacuated glass tube solar

collector. The thermal efficiency was around 40%. Evacuated tubes solar collectors are ideal and simple to incorporate with buildings. However, since the vacuum tube is filled with water, which increases the thermal mass of the collectors, the output in low ambient temperature seasons is low (Kumar, Said and Bellos, 2021). In order to get higher output, (Yang *et al.*, 2020) studied the performance of a micro parabolic trough concentrator coupled with an evacuated tube. The thermal efficiencies was found to be 37.55%. (Chenggang and Fei, 2020) proposed a building integrated Compound Parabolic Concentrator (CPC) coupled with both open evacuated tube. The average thermal efficiency was calculated as 51.4%.

According to literatures on building-integrated concentric collectors, the most commonly used receiver is water-in-glass evacuated-tube. These receivers are less expensive than metal-in-glass direct-flow evacuated tubes, but they have disadvantages including poor thermal output and being easily damaged by mechanical stress, especially in large-scale systems (Glembin, Rockendorf and Scheuren, 2010). This prompted the study of an Asymmetric Compound Parabolic Concentrator (A-CPC) coupled with a concentric aluminum tube heat exchanger inserted in an all-glass evacuated tube receiver. The proposed design reduces thermal stress throughout the evacuated tube and enhances heat transfer by creating a more uniform rate of heat transfer throughout the concentric tube. The research work will also serve as a foundation for future research on building-integrated solar collectors by demonstrating the viability and worthiness of considering vertically mounted solar collectors on building walls in low-latitude countries.

1.2. Statement of the Problem

According to IRENA statistics on global thermal energy demand for buildings, approximately 17 Exajoules is used for building water heating, with electricity accounting for 18% (3.06 Exajoules) (IRENA, 2020). The installed capacity of electric water heaters and the amount of energy required for water heating were 41.1 MW and 18.7 GWh/year, respectively, according to a survey on the thermal energy consumption of commercial buildings in Addis Abeba carried out in 2021 (PEA, 2021). In an effort to reduce this huge conventional energy consumption by buildings, solar thermal collectors have been introduced to the field of building energy conservation.

Solar thermal collectors, such as solar water heaters, are typically mounted on building rooftops. When there is adequate rooftop space to mount the collector, this method of installation is effective. However, rooftop space is limited in most high-rise buildings, while

hot water consumption is considerable due to the large number of dwellers. Another issue with rooftop installations is the need for long lengths of piping to supply hot water from the roof to each dwellings. This results in significant heat loss and the loss of a huge volume of cold water due to the pipe being drained before using the hot water. Additionally, the rooftop installation affects the building's aesthetics by being irregular, random, and unstructured (Aldegheri *et al.*, 2014; Buker and Riffat, 2015; Zhang *et al.*, 2015; Buonomano *et al.*, 2019).

Building walls are becoming a viable space for solar collector installation. The integration of conventional solar thermal collectors, such as FPCs and ETSCs, on building wall results in low energy outputs, which restricts their applicability. (Lee *et al.*, 2014) investigated the performance of building integrated FPC and found a thermal efficiency of 22.8%. An ETSC integrated onto a balcony was demonstrated to have a 40% thermal efficiency according to research by (Li, Dai and Wang, 2015).

A potential remedy for this low thermal efficiency issue is to install a fixed non-tracking solar concentrator on building walls. Therefore, this study aims to designing, manufacturing, and testing the performance of a building-integrated Asymmetric Compound Parabolic Concentrating solar collector to address the aforementioned problems. Furthermore, the study will address the viability of considering building-integrated solar thermal collectors in low-latitude countries such as Ethiopia.

1.3. Objective of the Study

1.3.1. General objective

The main objective of this study was to design, manufacture, and evaluation of the performance a building-integrated Asymmetric Compound Parabolic Concentrator (A-CPC) solar evacuated glass tube collector with concentric tube heat exchanger.

1.3.2. Specific objective

The specific objectives of this study are:

- To design optical geometry of building-integrated A-CPC based on solar altitude angle
- To simulate the optical performance of the collector for different incident angles by ray-tracing method using TracePro Software
- To manufacture and test the performance of the collector under real weather condition

1.4. Significance of the Study

The significance of this study can be absorbed from different perspective. First, implementing this study will reduce the huge consumption of conventional energy in buildings. Second, the thermal energy is generated at the point of use, which minimize the heat loss and lowers the total cost of producing thermal energy. Additionally, the implementation of this study will bring power demand reduction in buildings. This, in turn, enhances energy security and also provides monetized power costs as a result of decreased power demand. Furthermore, the proposed solution reduces the associated carbon footprint, especially for hotels and other commercial buildings that use fossil fuel boilers.

1.5. Scope of the Study

The study focuses on design, manufacture, and evaluation of the performance a building-integrated A-CPC solar evacuated glass tube collector with concentric tube heat exchanger. The optical geometry of A-CPC was developed using the standard CPC equation. TracePro, a ray tracing mk software, was used to simulate optical performance at various solar altitude angles. The proper materials that were available were used to manufacture the collector. The test is based on Ethiopian Standard ES-ISO 9806: 2015 for outdoor test procedures for system performance characterization. Water was used as the working fluid during the experiment.

1.6. Limitations

The primary focus of this research is on the thermal performance of the collector through experimental investigation. The thermal characteristics of the collector were not simulated. Even if the experiment is successfully carried out, the prototype may not be placed or integrated into the actual system / building/. However, the experimental findings of the study are validated by previous published articles in the area. The project scope is also limited by the available time and budget.

CHAPTER TWO
LITERATURE REVIEW

This chapter presents a detailed literature review on building-integrated solar thermal collectors. It address: the type and application of building-integrated concentrating solar thermal collectors, criteria for integrating solar thermal collectors into architecture, the suitability of building facades, and finally the performance of such collectors.

2.1. The need for building integrated concentrating solar thermal collectors

Buildings that are designated as eco-friendly structures cover their energy needs from renewable energy source. Concept of energy efficient buildings does not only mean the usage of insulating materials as building elements, but also use of renewable energy source in their concept. The most ecological and sustainable energy source to be integrated on the buildings is the solar energy systems for water and space heating (Ilija Nasov, 2015).

Solar thermal collectors are one of the most promising solar technologies for the aforementioned purposes. They capture solar energy from the sun, convert it to heat energy, and then transfer that heat to a heating medium like water, air, or oil. Thermal energy used to heat liquids may be utilized directly for several applications.

As a result, solar thermal collectors were traditionally installed on roofs rather than facades; however, this concept has shifted in the last couple of decades (Maurer, Cappel and Kuhn, 2017). First, due to the typical disorganized, random, and irregular installation of solar collectors on rooftops, this affects the appearance of the building. Second, due to the frequently inadequate ratio of available roof area to required solar collector area, it is challenging to supply enough energy from roof collectors to meet the entire energy needs of the buildings. In order to prevent the unsightly solar collectors and lower the price of building thermal energy consumption, the building integration of the solar collector system is an urgent necessity (Maurer, Cappel and Kuhn, 2017; Buonomano *et al.*, 2019; Chenggang and Fei, 2020).

To address this issue, the space on the facades might be exploited, particularly if there is adequate area on the building's south façade wall. The south face of the building might be more appealing or a better location for solar collectors (Harmim *et al.*, 2013; Xuan *et al.*, 2017; Gagliano, Aneli and Nocera, 2019).

Solar façade collectors also have the advantage of being less susceptible to environmental factors, since snow and dirt have little effect on their performance when positioned vertically (Frattolillo *et al.*, 2020).

Future net zero energy buildings will require high quality heating sources, particularly during the winter, for dehumidification, refrigeration, and space heating in addition to water heating (Muhammad-Sukki *et al.*, 2014). However, the applicability of the conventional flat solar thermal system is limited since it can only provide heat at low temperatures challenging due to low intensity radiation. In this regard, the installation of building integrated solar concentrating systems could fulfill the need for thermal energy in buildings. According to IRENA, IEA (2017), as cited by (Li, Xuan, M W Akram, *et al.*, 2020), building integrated solar concentrating systems has therefore been demonstrated to be effective despite any such constraints.

The concentrating solar thermal systems in this situation could be able to provide a solution. One of the key benefits of concentrating technology is that it can deliver heat resources at greater temperatures (Harmim *et al.*, 2013), making it more appropriate for use in buildings. Thermal collector systems that are part of a building are either incorporated into the structure's roof or its façade. They may be utilized in a way that renders them undetectable and visually pleasing depending on the kind and size of the collector (Chemisana, 2011).

2.2. Criteria for integrating solar thermal collectors into architecture

Solar thermal collectors must meet the following criteria in addition to being technically and structurally effective in order to be incorporated into buildings. The IEA Task 41 Solar Energy and Architecture proposed the following criteria, which are generalized in these guidelines, for the aesthetic value of buildings integrated solar thermal collectors (Wall *et al.*, 2012):

- Seamlessly integrating
- Elegant architectural design
- Material and color choices that is appropriate
- Size that complements the harmony and combo
- Fidelity to the building's surroundings
- Creative and well-balanced design

2.3. Suitability of building facades (Solar radiation on building façade)

Many studies have been conducted on amount and availability of solar radiation on building façade. (Brito *et al.*, 2017) investigated the potential of building facades and other vertical surfaces for the solar photovoltaic power generation in the city of Lisbon, Portugal. They used digital surface model determined from LiDAR (Light Detection and Ranging) measurements and local typical meteorological year time series. Study showed that, façade receive solar irradiation only from 100 to 1000 kWh/m^2/year. The higher annual irradiation is found on south facing facades and the lower on north facing facades. In contrast, roof surface receives much higher levels of solar irradiation, in the 1000 – 1800 kWh/m^2/year. Figure 2-1 (a) and (b) shows the maps of annual solar irradiation and solar potential histogram, respectively.

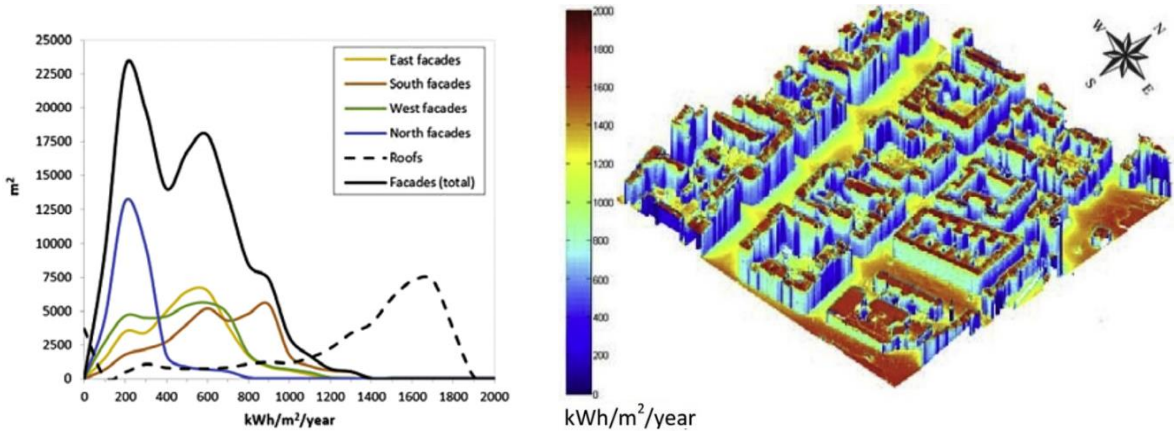

(a) (b)

Figure 2-1: Annual (a) solar potential histogram and (b) irradiation (Brito *et al.*, 2017)

(Desthieux *et al.*, 2018) also assessed solar radiation and energy production on building rooftops and vertical facades using LiDAR, 2D, and 3D cadastral data. They investigated the global irradiance for a set of points located on roofs, ground, and facades. They found out that facades are a potential candidate for solar energy production, especially during the winter months. Figure 2-2 shows the 3D representation of solar energy on building roofs and facades.

Many studies reveal that façade integrated collectors gives relatively more yield in winter season and less in summer season, and more in the early and late hours of the day, when the sun is lower in the sky (Redweik, Catita and Brito, 2013; Brito *et al.*, 2017; Kayali and Dr. Halil Alibaba, 2017).

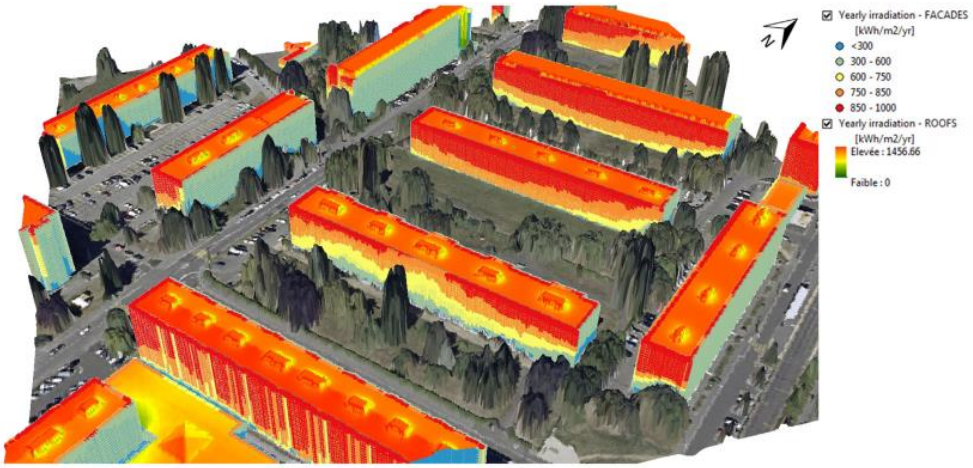

Figure 2-2: 3D representations of the solar radiation outputs on building facades and roofs in the Meyrin city (Boulmier (2016) as cited by Desthieux et al., 2018)

Figure 2-3 shows the comparison of the monthly solar radiation incident on 45^{o} south oriented tilted collector versus south oriented building façade in Graz, Austria.

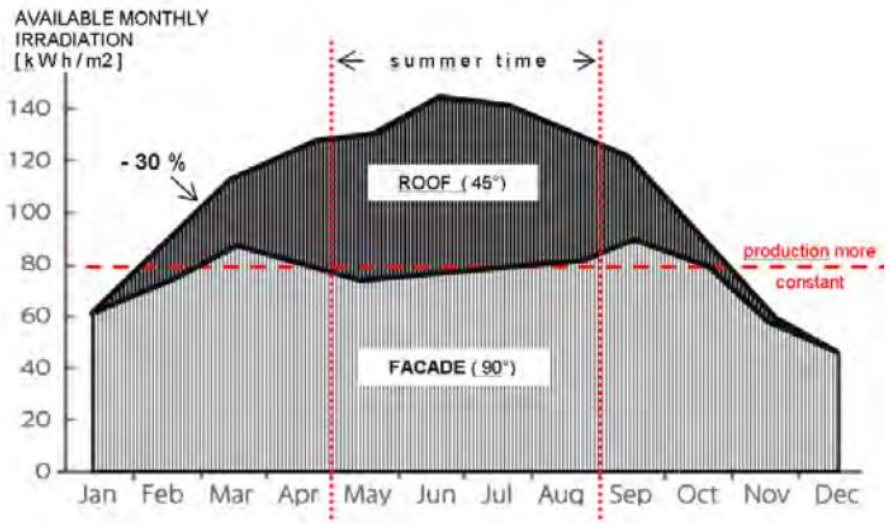

Figure 2-3: Roof versus facade collector annual yield pattern (Probst M (2008), as cited by Ilija Nasov, 2015)

The majority of studies on the potential of façades for solar energy system applications has been conducted in high-latitude countries. However, low-latitude countries also have the potential to deploy building-integrated systems on vertical surfaces. In contrast to high latitude countries, low latitude countries have high incidence angles but more annual energy is available on vertical surfaces. (Cronemberger, Caamaño-Martín and Sánchez, 2012) revealed that in low-latitude countries, the availability of solar radiation on vertical surfaces is nearly 60%.

2.4. Types and performance of building-integrated solar thermal collectors

There are several types of solar thermal collectors that are incorporated into building facades and may provide a variety of building services, including hot water delivery, building heating and cooling, and insulation enhancement. The building-integrated solar thermal collectors would increase building energy efficiency and effectively transform the envelope into a self-sufficient energy source.

2.4.1. Building integrated non-concentrating solar thermal collectors

(Visa, Moldovan and Duta, 2020) investigated solar thermal facades made up of nine innovative flat plate solar thermal collectors with trapezoidal shapes. When comparing specific thermal energy production, trapezoidal collectors have a specific energy output that is 28.72% less than commercial collectors. The results reveal that heat output is greatly influenced not only by the amount of solar radiation but also by the average external air temperature during the winter season.

(Buonomano *et al.*, 2019) presented a work on the thermodynamic performance of a novel flat-plate solar thermal collector, suitable for façade integration, with water as the heat transfer fluid. Their research indicates that the maximum primary energy savings and avoided CO_2 are 76.3 kWh/m^2 y and 850 kgCO_2/y, respectively.

(Lee *et al.*, 2014) assessed the annual performance of a near-zero-energy solar home built on the campus of the Korea Institute of Energy Research's flat plate solar water heating system integrated into the façade and solar photovoltaic (PV) modules installed on the roof. The annual efficiencies of the building's integrated solar thermal collectors and solar PV were 22.8% and 10.9%, respectively.

(Chow, He and Ji, 2007) tested the performance of a façade-integrated solar PV/thermal collector capable of serving as a water pre-heating system. The thermal efficiency was determined to be 38.9%, with an electrical conversion efficiency of 8.56 %. All-ceramic FPCs built of conventional ceramic and V-Ti black ceramic were investigated by (Yang *et al.*, 2013). It was designed to swap out for the building materials. For instance, they might serve as balcony railings. The thermal efficiency of solar thermal collectors acting as balcony railings is around 47.1 percent.

Furthermore, (Ji, *et al*., 2010) Published a paper on an innovative facade-integrated dual purpose solar collector system. The system has two distinct working modes: passive room heating and water heating. It operates in the passive room heating mode on cold days like winter days, while in warm months like summer, it operates in the water heating mode.

Table 2-1: Summary of previous studies on building-integrated FPCs

References	Structure	Type of Collector	Type of Study	Remarks and Key Findings
(Chow, He and Ji, 2007)		• Flat PV/T	• Experimental	• The thermal efficiency was determined to be 38.9%, with an electrical conversion efficiency of 8.56 %.
(Lee *et al.*, 2014)		• Flat Plate Collector	• Experimental	• The annual efficiencies of the building's integrated FPCs and solar PV were 22.8% and 10.9%, respectively.
(Buonomano *et al.*, 2019)		• Flat Plate Collector	• Experimental • Simulation	• The highest primary energy savings (76.3 kWh/m2/y) and prevented CO2 emissions (about 850 kgCO2/y) were realized.
(Visa, Moldovan and Duta, 2020)		• Trapezoidal collector	• Experimental	• The new collectors have a specific thermal energy that is 28.71 percent lower than the FPC. • This disadvantage might be mitigated by increasing the collector area on the façade of a given building.

(Li, Dai and Wang, 2015) developed a new design for a household solar hot water system used in high-rise buildings. They devised and built a U-shaped evacuated glass tube solar collector that is installed vertically on the balcony wall. The average daily collector efficiency, as determined by the experimental findings, is around 40%.

Figure 2-4: Appearance of the evacuated tube solar water heater integrated in the building (Li, Dai and Wang, 2015)

The effect of installation position on the performance of evacuated glass U-tube solar collectors has been investigated by (Ong, Tong and Choong, 2016). From the results, they found that the evacuated glass U-tube solar collectors performed better when installed in an inclined position than when installed vertically (balcony installation).

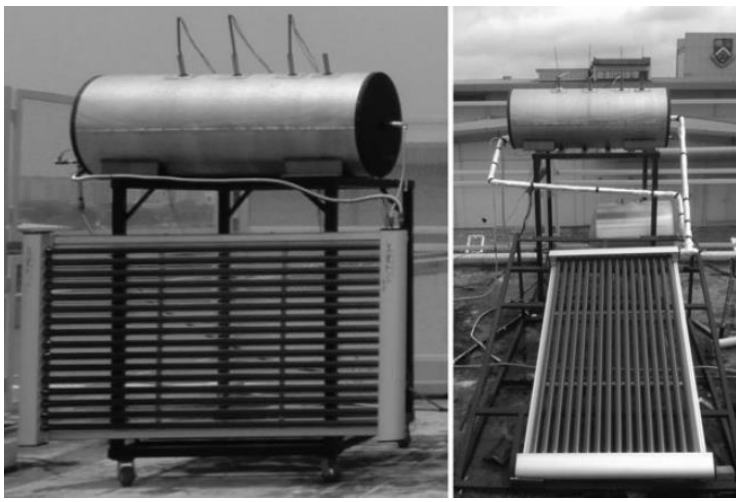

Figure 2-5: Experimental setup of U-tube evacuated glass tube solar water heater with vertical and inclined panels (Ong, Tong and Choong, 2016)

In a review article regarding vacuum-tube based building-integrated solar thermal systems (Lamnatou *et al.*, 2016), it was highlighted that glass evacuated-tube collectors offer greater benefits than flat-plate collectors. The review paper also disclosed that a vacuum-tube collector and a CPC reflector may be coupled. High temperatures may thus be obtained even throughout the cold season (with low outside temperatures).

The benefits of vacuum-tube collectors, according to Comerford (2011), as cited by (Lamnatou *et al.*, 2016), include:

- Compared to flat-plate collectors, they have a larger solar yield (with the same collector area).
- They have minimal heat losses and are 30% more effective than flat-plate collectors.
- Their capacity to work in windy, humid and cold environments.
- The ability to rotate individual tubes in order to maximize the optimal alignment.
- Their capability to achieve high temperatures.
- The collector is impervious to moisture and dirt (since the vacuum-tube is sealed).

Table 2-2: Summary of previous studies on building-integrated ETSCs

References	Systems	Type of ETSC	Type of Study	Remarks and Key Findings
(Li, Dai and Wang, 2015)	• Balcony wall-integrated water heating in high-rise buildings	• Two layered glass U-tube evacuated tube (vertical arrangement)	• Experimental • Simulation	• Average daily collector efficiency 40% • Annual solar fraction 40.5%
(Ji *et al.*, 2015)	• Two sets of balcony-type FPCs and two sets of balcony-type ETSCs	• Water in glass ETSC	• Experimental	• The temperature rise was 24.6-28.2 ^{o}C with an initial temperature of 13 ^{o}C and a solar radiation of 16.5 MJ, and the efficiencies were about 60%.
(Zhang *et al.*, 2015)	• Review about building integrated solar thermal technologies and their applications	-	-	• Since ETSCs are lighter, more efficient, and easier to assemble and connect pipes, they have more prospective applications in balcony-based integration.
(Ong, Tong and Choong, 2016)	• Balcony-type and inclined collector panel solar water heating systems	• Two layered glass U-tube evacuated tube (horizontal arrangement)	• Experimental	• For the balcony-type system, the temperature rise is 35 ^{o}C. • Comparing the two collector types, the inclined collector performed better.
(Lamnatou *et al.*, 2016)	• Review about vacuum-tube-based building-integrated solar thermal systems	-	-	• Evacuated tubes are recommended for building integration. • Whereas FPCs seem promising for roof-based installations.

2.4.2. Building integrated concentrating solar thermal collectors

The integration of traditional solar thermal collectors such as FPCs and ETSCs on buildings may result in low energy outputs, lead to relatively low hot water temperature, limiting its applicability. In this instance, concentrated solar thermal systems may be a viable alternative. They have a number of advantages over conventional collectors, the three most significant of which are that they permit a more flexible use of space (Chemisana, 2011), produce more energy per square meter (Aldegheri *et al.*, 2014), and offer thermal energy at a higher temperature (Li, Xuan, M. W. Akram, *et al.*, 2020).

(Ulavi, Hebrink and Davidson, 2014) investigated a hybrid "solar window" that provides heating as well as daylighting. The system consists of a CPC with a wavelength-selective film, as illustrated in Figure 2-6. The developed system transmits the visible portion of the incident solar spectrum into the interior area. To gather thermal energy, the infrared spectrum is reflected and focused onto the tubular absorber. According to the simulation results, the collector may reach thermal efficiencies of 18 and 24 percent at acceptance angles ranging from -25 to 45 degrees, respectively. The corresponding concentration ratio ranges from 2.6x at a 25^{o} acceptance angle to 1.5x at a 45^{o} acceptance angle.

An innovative non-tracking box-type solar cooker that is equipped with an asymmetric CPC as a booster-reflector has been introduced by (Harmim *et al.*, 2013). As depicted in Figure 2-7, the concentrator of the cooker is attached to the south wall of the building, while the rear opining section is in the kitchen, making it more user friendly. The solar altitude angel that the collection receives ranges from 27.5° to 85°. Because of the wide range of solar altitude angles, the cooker can work for at least 5 hours per day. 2× is the collector's maximum concentration at a 60^{o} acceptance angle. The optical efficiency was as high as 92.7 percent, indicating that the solar radiation was efficiently used. The highest absorber-plate temperature reached 166 ℃ during no-load test.

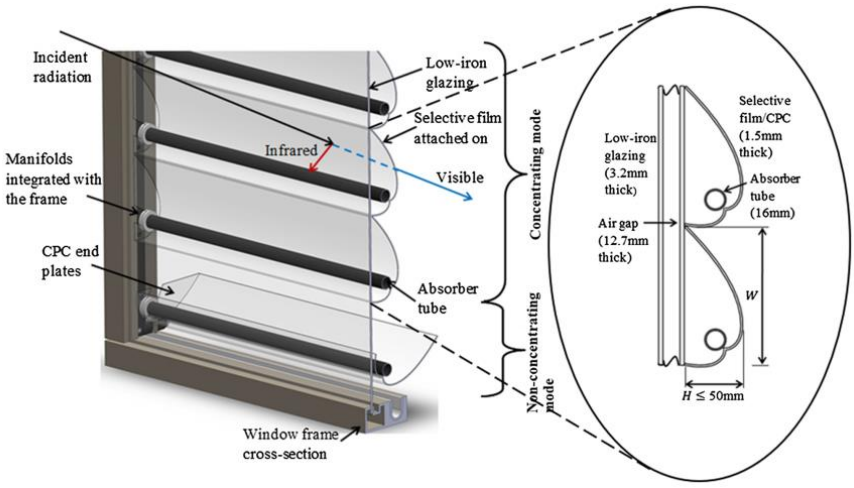

Figure 2-6: Schematic representation and cross sectional view of hybrid solar window (Ulavi, Hebrink and Davidson, 2014)

(a) (b) (c)

Figure 2-7: (a) Façade integrated solar cooker prototype, (b) interior side and (c) external side (Harmim *et al.*, 2013)

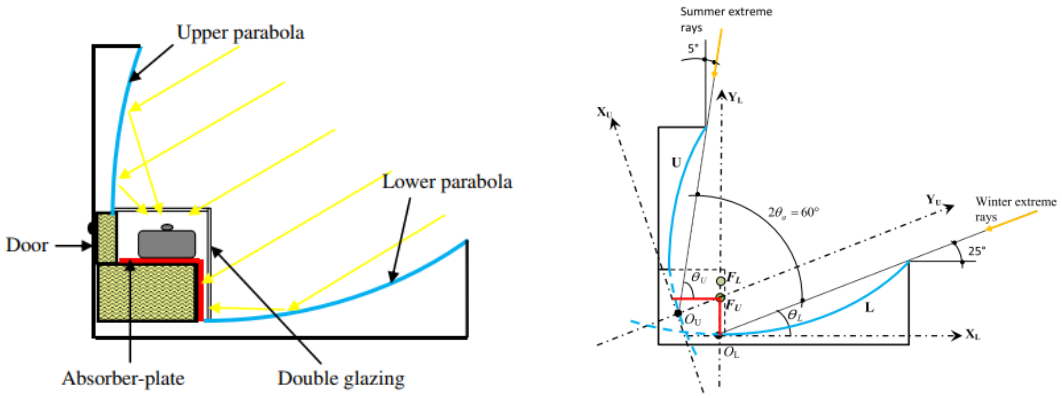

(a) (b)

Figure 2-8: (a) Schematic skated of façade integrated solar cooker and (b) geometry of asymmetric CPC for façade integrated solar cooker (Harmim *et al.*, 2013)

(Deng and Chen, 2020) have designed, fabricated and tested have tested a novel façade embedded CPC collector paired with an evacuated tube collector that is suited for integration into building vertical walls, balconies, and other similar structures. Figure 2-9 depicts the schematic diagram of the system that is attached to the building's south façade. The CPC has been tangent-truncated, and its geometric concentration ratio is $2.39\times$ with a half acceptance angle of 31.8^{o}. The Monte-Carlo Ray-Trace technique was used to assess optical efficiency. It was discovered that the optical efficiency was 64.5% on average. The results of the experimental tests revealed that the thermal efficiency at its maximum and average levels is 55.4% and 51.4%, respectively.

(Mboup, Nakayama and Akisawa, 2020) have reported a wall-mounted concentrating solar collector that combines evacuated glass tubes with parabolic and involute reflectors to boost solar energy collection for domestic hot water heating system during winter. Figure 2-10 depicts the device's cross-sectional and 3D views. TracePro software, a ray tracing program that employs the Monte Carlo ray tracing approach, was used to conduct the simulation study. The investigation showed that the highest amount of energy gathered was 5.5 times greater than the amount of energy gathered when the receiver is positioned alone without the reflector.

(Yang *et al.*, 2020) investigated numerically and experimentally the optical and thermal performance of a micro parabolic trough concentrating collector for building integration. Figure 2-11 and Figure 2-12 show the suggested design, which comprises evacuated tube receivers and a tracking system. Due to the lack of small size evacuate tubes, the copper tube was used in place of the evacuate tube receiver during the experimental test. The design achieves a concentration ratio of 4.2 in a collector thickness of 150 mm, making the system small enough to be incorporated with building rooftops and façades. The system's annual optical and thermal efficiencies was estimated to be 0.667, while its thermal efficiency at 200 °C was estimated to be 0.593. The numerical model also predicted that the system's optical and thermal efficiencies would be 0.441 and 0.375, respectively, if it were installed on a building's vertical walls.

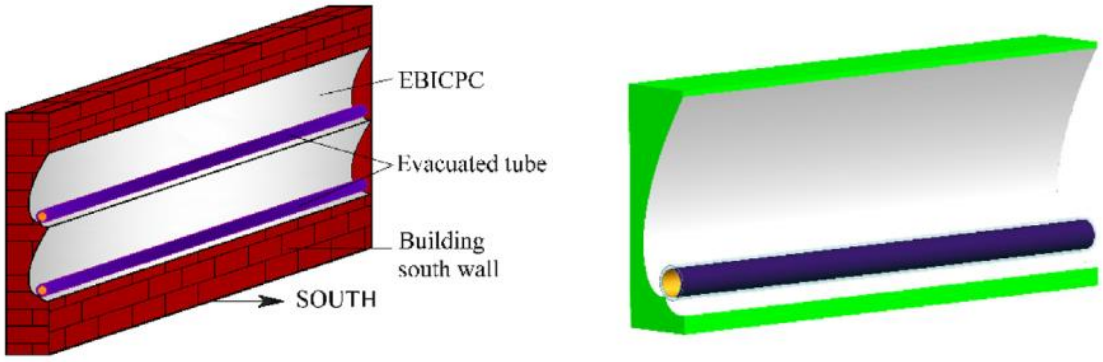

(a) (b)

Figure 2-9: (a) south façade integrated solar collector and (b) 3D model of façade integrated CPC (Deng and Chen, 2020)

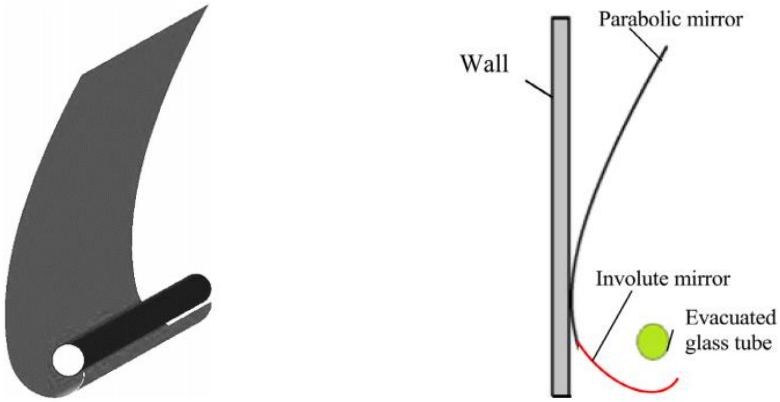

(a) (b)

Figure 2-10: (a) 3D view and (b) cross sectional view of the wall mounted solar concentrating collector (Mboup, Nakayama and Akisawa, 2020)

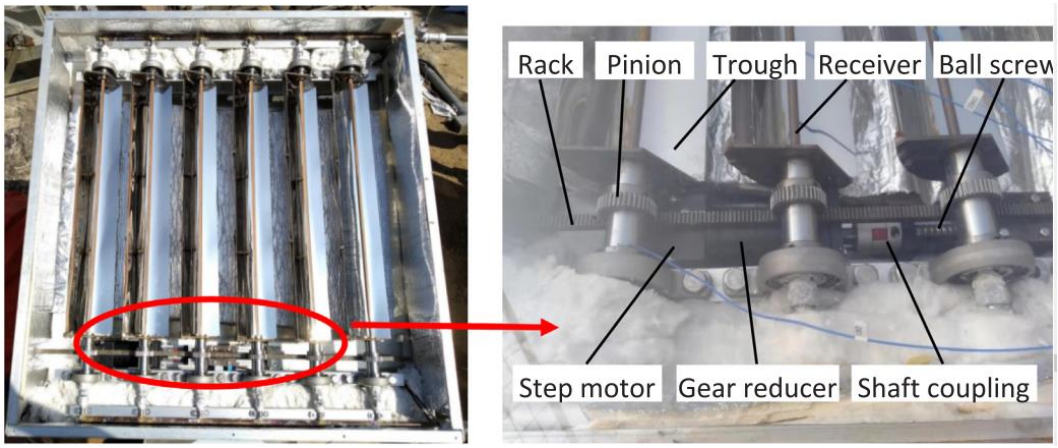

Figure 2-11: Prototype of micro-parabolic concentrator with tracking mechanism (Yang *et al.*, 2020)

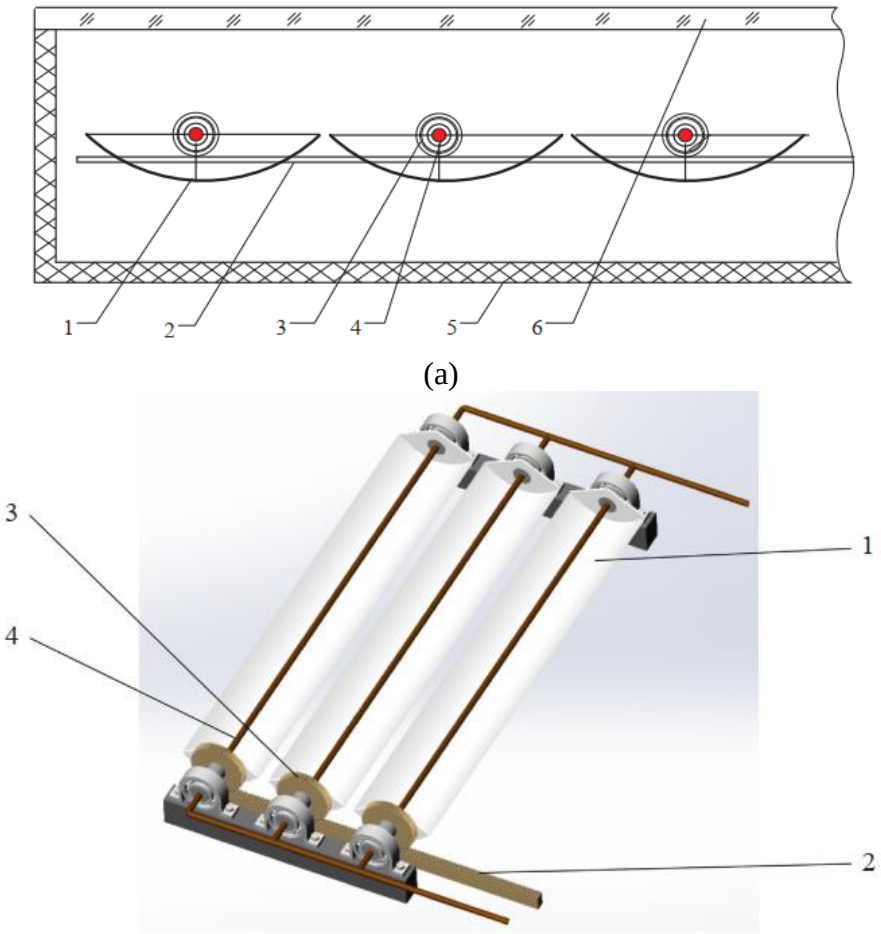

Figure 2-12: Schematic of the designed micro-parabolic concentrator (a) Sectional view and (b) 3D view (excluding glass cover and frame) 1- micro-parabolic troughs, 2- rack, 3-pinion;,4 – receivers, 5 – body and insulation and 6 - glass cover (Yang *et al.*, 2020)

(Harmim *et al.*, 2019) designed and tested a novel integrated linear parabolic reflector storage solar water heater for vertical building wall integration. The 3D view of the designed system is shown in Figure 2-13. The device has two purposes: it concentrates solar radiation and stores heat during the winter and ventilates the building's interior during the summer. The concentrator surface is an assembly of small rectangular and pivoting reflectors. When the device is used as ventilator during summer, this reflector is pivoted to horizontal position. The range of solar altitude angel intercepted by the collector is from 25^{o} to 85^{o}. 3.3× is the geometric concentration ratio of the collector. The test results revealed that the highest water temperature attained varied from 40 to 49 degrees Celsius depending on the weather situations. The average daily efficiency ranges between 36.4 and 51.6 percent, while its thermal losses coefficient at night is between 2.17 and 3.12 WK^{-1}.

(a) (b)

Figure 2-13: 3D view of integrated storage SWH: (a) External side in winter period and (b) Internal side when the SWH is not used (Harmim *et al.*, 2019)

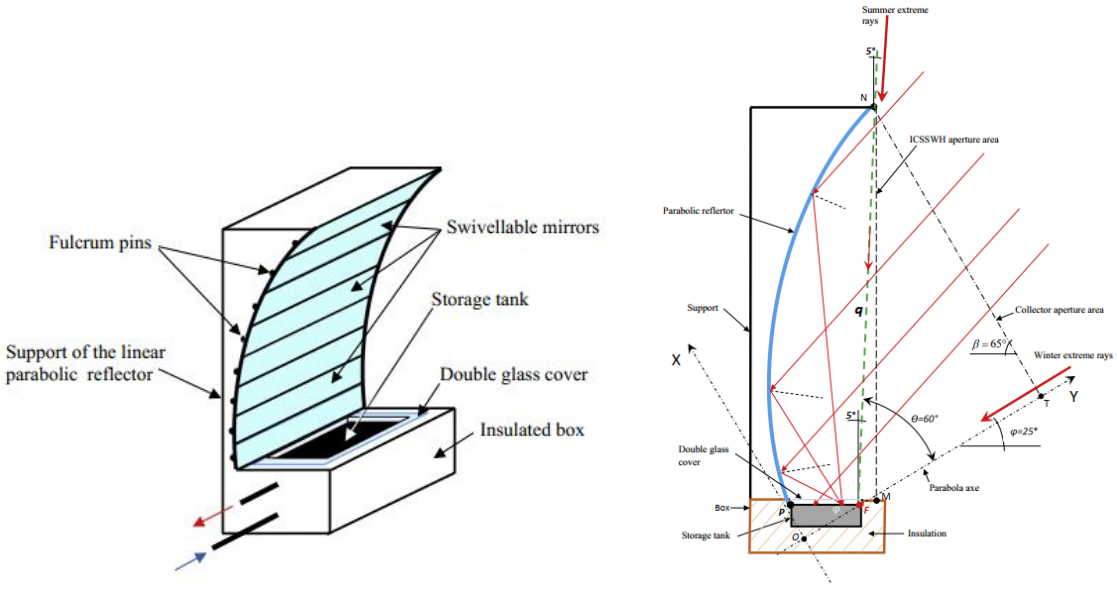

(a) (b)

Figure 2-14: Schematic diagram of integrated storage SWH equipped and (b) Geometry of the linear parabolic reflector (Harmim *et al.*, 2019)

Table 2-3: Summary of previous studies on building integrated concentrating solar thermal collectors

References	Key features	Working fluid	Concentrator type	Concentration ratio	Acceptance range	Highest temperature	Thermal efficiency	Optical efficiency
(Harmim *et al.*, 2013)	The system consists of a line-axis asymmetric CPC as a booster-reflector and an absorber-plate.	-	Asymmetric CPC	2	27.5º to 85º	-	-	92.7%
(Ulavi, Hebrink and Davidson, 2014)	The integration of a wavelength selective film and a CPC.	Ethylene glycol 40%	Asymmetrically truncated CPC	1.5 to 2.6	25º to 45º	-	18 to 24%	-
(Kashiide, Akisawa and Enoki, 2015)	Consists of a linear parabolic mirror for concentration and a flat receiver constructed of serpentine copper tube coated in chrome.	Water	Linear parabolic reflector	-	-	45.8 ºC	-	-
(Harmim *et al.*, 2019)	A new integrated collector storage solar water heater equipped with linear parabolic mirror constructed from small rectangular and pivoting reflectors.	Water	Linear parabolic reflector	3.3	25º to 85º	49 ºC	36.4 to 51.6%	-
(Chenggang and Fei, 2020)	A CPC collector as the concentrator and both sides open evacuated tube as the receiver.	Water	Asymmetrically truncated CPC	2.39	24.9º to 88.6º	76 ºC	51.4%	64.5%
(Mboup, Nakayama and Akisawa, 2020)	Consisting of a parabolic and involute reflector, as well as a U-tube evacuated tube.	Water	Parabolic and involute reflector	5.5	Not considered	-	-	-
(Yang *et al.*, 2020)	A combination of parallel micro-parabolic troughs, evacuated tube absorbers (8 mm outer diameter), and an internal tracking mechanism.	A synthetic organic oil (Diphyl DT)	Micro-parabolic trough collector	4.2	-	200 ºC	37.5%	44.1%

2.5. Modes of Solar Collector Installation on Building Walls

(Huang *et al.*, 2019) have reported various methods of mounting solar collectors on building walls. According to their review, a wall-mounted collector can be installed in both vertical and tilted configurations. Figure 2-15 depicts various solar collector installation methods on a building wall. According to their findings, the Type 4 installation method offers the highest level of safety and efficiency for high-rise buildings. While type 2 is found to be non-conducive to the maintenance of the collector, types 1 and 3 installation modes pose a significant security risk.

Figure 2-15: Techniques of mounting a solar collector on building walls (Huang *et al.*, 2019)

Types	Type 1: attached	Type 2: embedded	Type 3: Bracket	Type 4: Pallet
Sketches		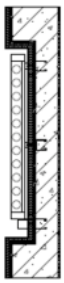	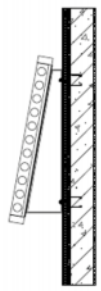	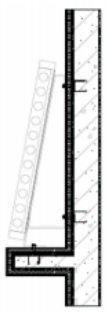
Installation mode	Attached to wall	Embedded in the wall	Attached to the wall by a stainless-steel bracket	Supported by a pallet
Angle	0º	0º	15º	15º
Cases for FPCs				
Cases for ETCs				

2.6. Design Considerations of Cylindrical Absorber CPC

2.6.1. Truncation of standard CPC

The disadvantages of the standard CPC, particularly with a narrow acceptance angle, include: (a) the acceptance angle limits the effective operational period throughout the day (Yang *et al.*, 2020); and (b) the high cost of material utilization since ideal CPCs are extremely long, which results in high material costs (Isa, Rahman and Goh, 2015), etc. As a result, CPC is truncated to minimize its height, resulting in material, space, and cost savings with little or no reduction in performance. According to (Ustaoglu *et al.*, 2018), a CPC with a truncation level of 50% provides preferred performance with just a 1% drop in thermal performance and a considerable reduction in material demand.

The relation between truncation ratio, acceptance angle, and concentrating ratio was reported by (Yu, L. (2011) as cited by Jiang *et al.*, 2020). Figure 2-16 shows that the concentration ratio is significantly influenced by the truncation ratio, which decreases with increasing truncation ratio.

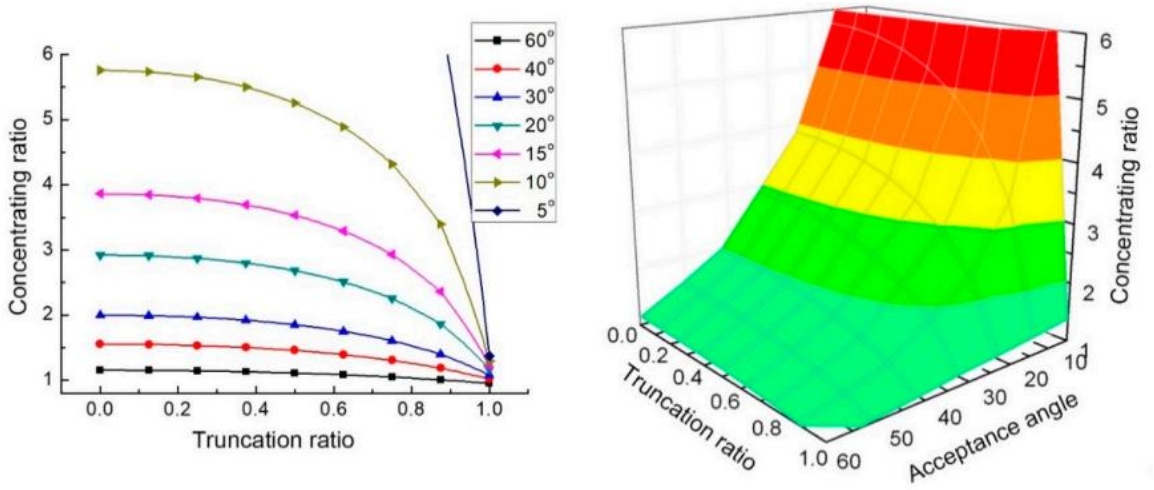

Figure 2-16: Relationship between truncation ratio, acceptance angle, and concentrating ratio (Yu, L. (2011) as cited by Jiang et al., 2020)

2.6.2. Absorber and flow path of the working fluid

The CPC collector may be divided into three subcategories depending on the absorber or flow channel of the working fluid: (1) CPC with heat-pipe, (2) CPC with U-tube pipe, and (3) CPC with coaxial pipe.

a) CPC with heat-pipe

Figure 2-17 shows a CPC with an evacuated tube heat-pipe attached to a cylindrical shaped aluminum fin (Pradhan, Mitra and Neogi, 2016). Its simplicity makes it a popular form of absorber for low temperature applications. Size and condenser efficiency are the two elements that affect the efficiency of the heat-pipe.

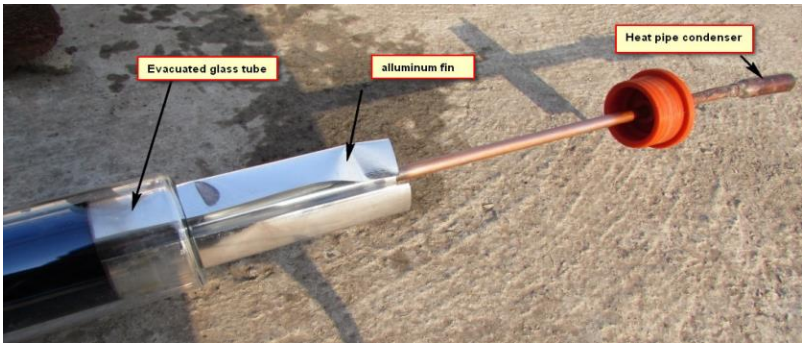

Figure 2-17: Depiction of a heat-pipe with evacuate tube (Pradhan, Mitra and Neogi, 2016)

b) CPC with U-tube Pipe

The schematic of an evacuated collector coupled with U-tube pipe is shown in Figure 2-18. It is made up of a copper or aluminum fin, an evacuated tube, and copper pipe with a U shape. Experimental comparisons between a water-in-glass evacuated tube and a U-tube evacuated tube were made by (Gao *et al.*, 2013). When comparing water-in-glass absorber to U-tube absorber, it was found that about 30% of the obtained energy was lost to the environment.

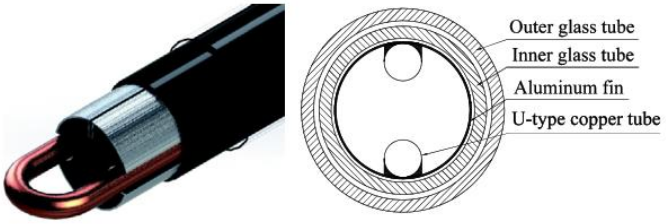

Figure 2-18: Schematic of evacuated U-tube solar collector (Nie *et al.*, 2017)

c) CPC with Coaxial Pipe

Figure 2-19 shows a typical CPC with an evacuated glass tube receiver with a coaxial pipe heat exchanger inserted inside. The design has a number of advantages over heat pipes, such as reducing thermal stresses in the tubes by keeping a consistent temperature differential as well as a uniform rate of heat transfer throughout the heat exchanger.

(Wang, Li and Liu, 2015) experimentally studied the performance of a new all-glass evacuated tube solar air collector with standard CPC and coaxial pipe heat exchanger. Table 5 summarizes the characteristics of different cylindrical absorber CPC collectors.

Figure 2-19: Photograph of CPC collector with coaxial pipe (Wang, Li and Liu, 2015)

Table 2-4: A summary of the characteristics of various cylindrical absorbers CPC

Types of Absorber	Advantage	Disadvantage
CPC with heat-pipe	• Structure adaptability • Simple to replace • Minimal thermal resistance • Anti-freezing	• High cost
CPC with U-tube pipe	• Easy structure • Low price	• Slightly high flow resistance • Slightly high thermal resistance • Not appropriate for internal CPC
CPC with Coaxial pipe	• Low thermal stress • Uniform heat transfer rate	• High flow resistance • Easy to block • Not suitable for internal CPC

2.6.3. Effects of gap between the absorber and the concentrator

To prevent thermal stress, which has the potential to distort the reflector, and to prevent thermal loss owing to conduction, a gap between the absorber and reflector could be necessary. This gap will, however, lower the concentration ratio and result in some solar radiation loss.

(Rabl, Goodman and Winston, 1979) suggested three different configurations for the CPC gap: Figure 2-20 (a) Minimizing the size of tubular receiver, Figure 2-20 (b) trimming the corners, and Figure 2-20 (c) changing the shape of receiver. In practice moving up the receiver is a frequent practice in actual design Figure 2-20 (d).

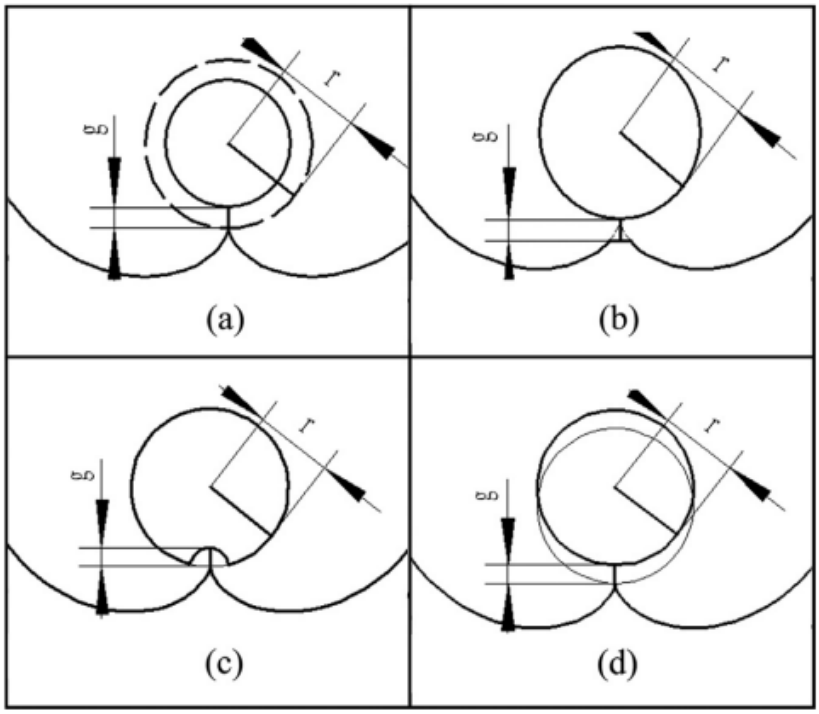

Figure 2-20: Four different methods of creating gaps in CPC (Wang *et al.*, 2016)

2.6.4. Effects of absorber radius and acceptance angle

Using ray tracing, (Abdullahi *et al.*, 2017) evaluated the effect of absorber radius and acceptance angle on the optical performance of a CPC collector. Nine distinct simulations were conducted with three acceptance angles (60^o, 40^o, and 30^o) and three absorber radii (25, 22.5, and 12.5 25mm). According to the results, the higher the acceptance angle, the higher the performance but the lower the concentration ratio. Furthermore, the results revealed that the smaller the absorber radius, the higher the performance for a given acceptance angle.

2.7. Research Gap

A comprehensive literature review was conducted by reviewing more than 60 published articles, studies, theses, and conference papers in the past 10 years. The literature review reveals that building-integrated solar thermal collectors are regarded as promising technologies and could transform the building façade from a passive to an active building element.

Many research have been done on building-integrated solar collectors. (Lee *et al.*, 2014) developed a wall mounted flat plate collector. (Li, Dai and Wang, 2015) developed a balcony mounted U-shaped ETSCs. ETSCs are ideal and simple to incorporate with buildings. However, since the vacuum tube is filled with water, which increases the thermal mass of the collectors, the output in low ambient temperature seasons is low (Kumar, Said and Bellos, 2021). In order to get higher output, (Yang *et al.*, 2020) studied the performance of a micro parabolic trough concentrator coupled with an evacuated tube. (Chenggang and Fei, 2020) proposed a building integrated system that comprise Compound Parabolic Concentrator (CPC) and both open all-glass evacuated tube.

The literature review showed that there exists study on Asymmetric Compound Parabolic Concentrating (A-CPC) thermal collectors that use both open all-glass evacuated tubes (water-in-glass) as receivers. These receivers are less expensive than metal-in-glass direct-flow evacuated tubes, but they have disadvantages including poor thermal output and being easily damaged by mechanical stress, especially in large-scale systems (Glembin, Rockendorf and Scheuren, 2010).

On reviewing the literatures, no research has yet integrated a concentric aluminum tube heat exchanger into the one-ended all-glass evacuated tube receiver with A-CPC for solar thermal collecting and evaluated the collector's performance experimentally. This prompted the study of an A-CPC coupled with a concentric aluminum tube heat exchanger inserted in an all-glass evacuated tube receiver. The proposed design reduces thermal stress throughout the evacuated tube and enhances heat transfer by creating a more uniform rate of heat transfer throughout the concentric tube. The research work will also serve as a foundation for future research on building-integrated solar collectors by demonstrating the viability and worthiness of considering vertically mounted solar collectors on building walls in low-latitude countries.

CHAPTER THREE
MATERIALS AND METHODS

This chapter presents the methodology and materials utilized in this study. The materials utilized to construct the system, as well as their corresponding properties, are provided in the material selection section. The methodologies used to develop the system are presented in the methods section. First, the methods for designing the Compound Parabolic Concentrator (CPC) collector's geometry are discussed. The optical evaluation approach is then explained to evaluate the CPC's optical performance. In-depth explanations are provided on the fabrication processes for the CPC. Finally, the performance evaluation approach for the proposed collector is discussed. Furthermore, detailed information on the measuring instruments, test setup, and measuring instrument calibration is provided to assure the proper function of the measuring instruments and the reliability of the experimental data.

3.1. Materials and Measuring Instruments

3.1.1. Materials

a) Reflector

Reflective Mylar RF015, a commercial reflective film, was selected. It has several characteristics such as high retro-reflection, outstanding silver surface, and thermo-stabilization, and is the ideal alternative for stainless steel and aluminum products. It also has a high quality and strong specular reflectance, with a reflectivity of 0.95.

Figure 3-1: Self-adhesive reflection Mylar (RF015)

b) Evacuated Tube

The dimension and surface properties of the borosilicate glass evacuated tube collector is shown in Table 3-1.

Table 3-1: Thermophysical properties of glass evacuated tube (Ma *et al.*, 2010; Naik and Muthukumar, 2019)

Material	Parameters	Value
Glass envelope	Outer diameter (m)	0.058
	Thickness (m)	0.002
	Conductivity (W/mK)	1.2
	Length (m)	1.8
Inner glass coating	Absorptance	0.93
	Reflectance	0.063
Inner glass	Outer diameter (m)	0.047
	Thickness (m)	0.002
	Conductivity (W/mK)	1.2

c) Concentric tube heat exchanger

The thermal conductivity, cost, and density of the material are taken into consideration while choosing the coaxial fluid conduit material. Typically, copper or aluminum is chosen because of their excellent heat conduction abilities. Because of the high cost and density of copper, aluminum is selected instead. The thermal conductivity value of aluminum is 236 W/mK (Li *et al.*, 2013).

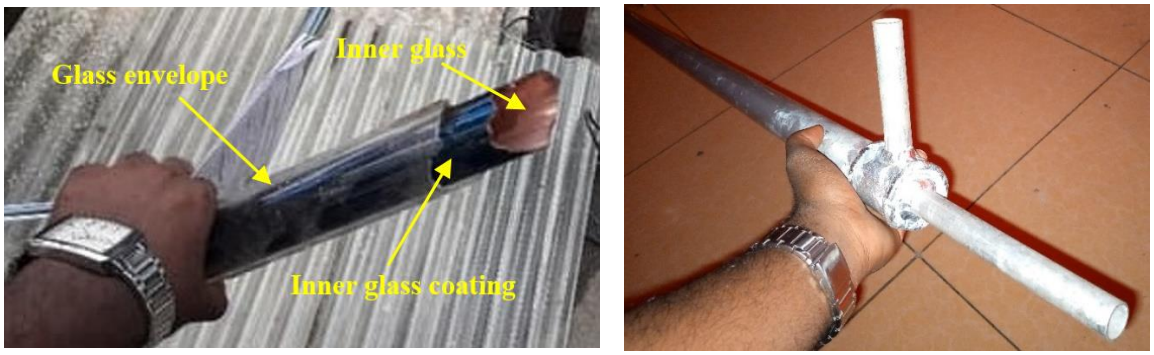

(a) (b)

Figure 3-2: Photograph of (a) All-glass evacuated tube and (b) Concentric tube heat exchanger used in this study

The solar receiver consisting of two welded and sealed aluminum pipes embedded in an all-glass evacuated tube. The outer and inner pipes of the concentric tube heat exchanger have respective outer diameters of 40 and 16 millimeters, and their thicknesses are 1.5 and 0.5 millimeters, respectively. Figure 3-3 depicts the concentric tube heat exchanger embedded in the all-glass evacuated tube.

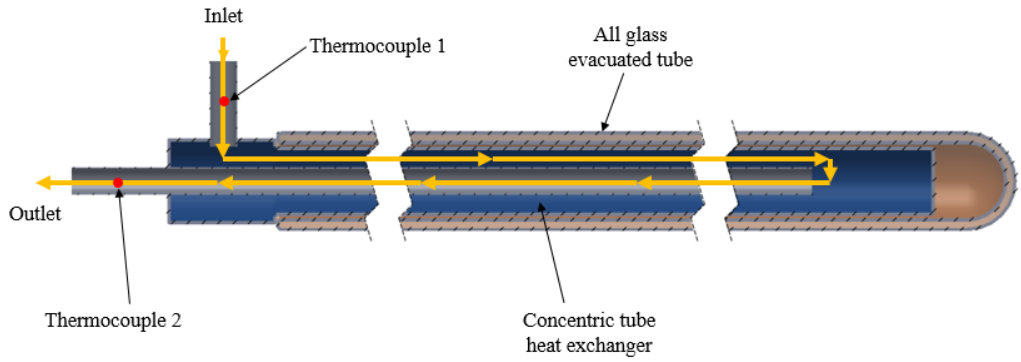

Figure 3-3: Structure of the concentric tube heat exchanger

d) Insulation Material for pipe and tanker insulation

To prevent heat loss from the pipe system and tank, 1.5 cm thick fiberglass insulation is used. At 80 degrees Celsius, the thermal conductivity of fiberglass is 0.035 W/mK (Dineshkumar, 2016).

3.1.2. Measuring devices and instruments

a) Solar radiation measurement

The CM3 pyranometer is used to measure the global solar irradiance on horizontal plane. The CM3 meets all requirement of the ISO-9060 pyranometer performance criterion. The Eppley radiometer, type PSP, is another instrument used to measure global solar radiation on the aperture plane. The specifications of the pyranometers is presented in Table 3-2.

(a) (b)

Figure 3-4: Photograph of (a) CM3 and (b) Eppley pyranometers used in this study

Table 3-2: Specification of CM3 pyranometer and PSP pyranometer

Parameters	CM3 pyranometer	PSP pyranometer
Light spectrum waveband	305 to 2800 nm	295 to 2800 nm
Maximum irradiance	2000 W/m^2	2800 W/m^2
Signal output	0 to 50 mV	0 to 10 mV analog
Sensitivity	22.5×10^{-6} VW^{-1}m^2	8.89×10^{-6} VW^{-1}m^2
Uncertainty	$\pm2\%$	$\pm1\%$

b) Temperature measurement

i) Collector inlet and outlet temperature

Digi-Sense Detachable Thermocouple Probe, produced by Cole-Parmer, is used to measure the temperature of the working fluid at the collector's inlet and outlet with an accuracy of $\pm0.4\%$ reading above 100℃ and $\pm2\%$ reading between -50 to 99℃. The instrument has an operating temperature of -150 to 427℃. The photograph of the instrument is shown in Figure 3-5 (b).

ii) Ambient temperature

Extech Instruments 407113 CFM Thermo-Anemometer is used measure the ambient air temperature with an accuracy of ±0.8℃. The instrument has an operating temperature of 0 to 80℃. The photograph of the instrument is shown in Figure 3-5 (a).

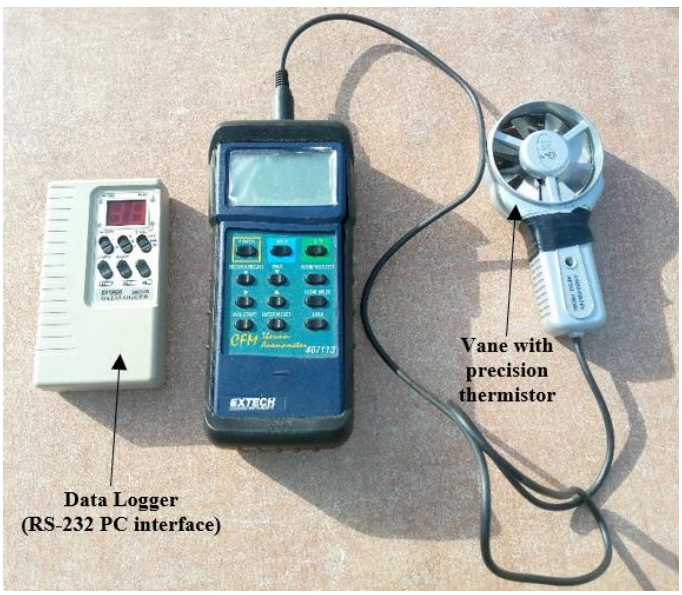

(a)

(b)

Figure 3-5: Photograph temperature measuring instruments used in this study (a) Extech Instruments CFM Thermo-Anemometer and (b) Detachable Thermocouple Probe

c) Data recorders

i) Data acquisition system

The National Instruments NI cDAQ-9172, a six-slot data acquisition system is used to record and save the recorded data every five minutes. The photograph of the data acquisition system is shown in Figure 3-6.

Figure 3-6: Photograph of NI cDAQ-9172 data acquisition system used in this study

The data acquisition process, including signal generation, signal processing, input-output control, and other operations, is programmed using LabVIEW, a graphical programming language. Figure 5.2 below illustrates the block diagram used in this study. The software was configured to log the data every five minutes.

LabVIEW, a graphical programming language, is used to create program the data acquisition process including signal generation, signal processing, input-output control and other functions. The front panel and block diagram used in this study is shown in Figure 5.2 below. The program was set to record the data every five minutes.

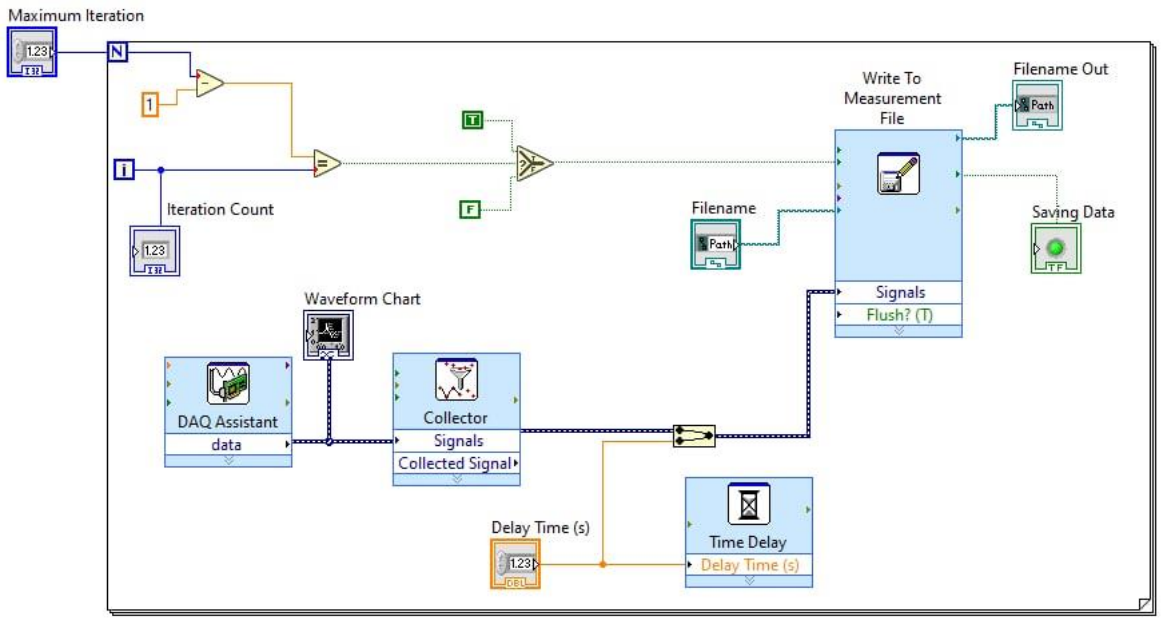

Figure 3-7: LabVIEW block diagram of the data acquisition system

ii) Eppley electronic-integrator

The Eppley electronic-integrator is used to provide a readout of the total amount of solar energy collected over a specified period.

(a) (b)

Figure 3-8: Photograph of Eppley electronic-integrator used in this study

d) Water pump and power supply

PM-5KPA-0.7L type water pump with PULS ML50.101 24VDC 2.1A power supply was used, shown in Figure 3-9. The flow rate is manually regulated using valves.

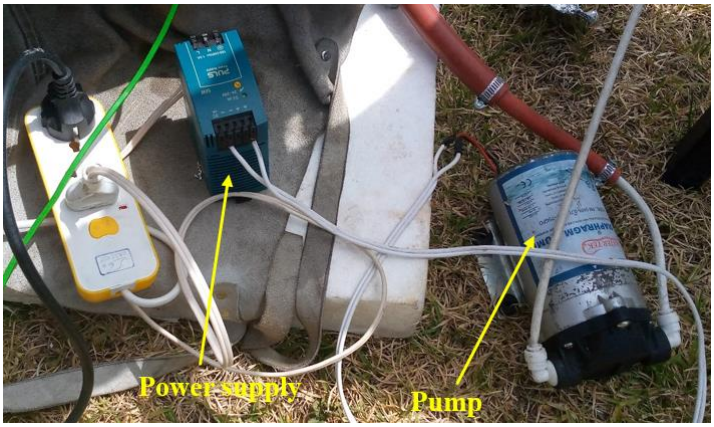

Figure 3-9: Photograph of the water pump and the power supply

3.2. Methods

A standard research method has been used to fulfill the objective of the study, as outlined in Figure 3-10, which begins with a detailed literature review.

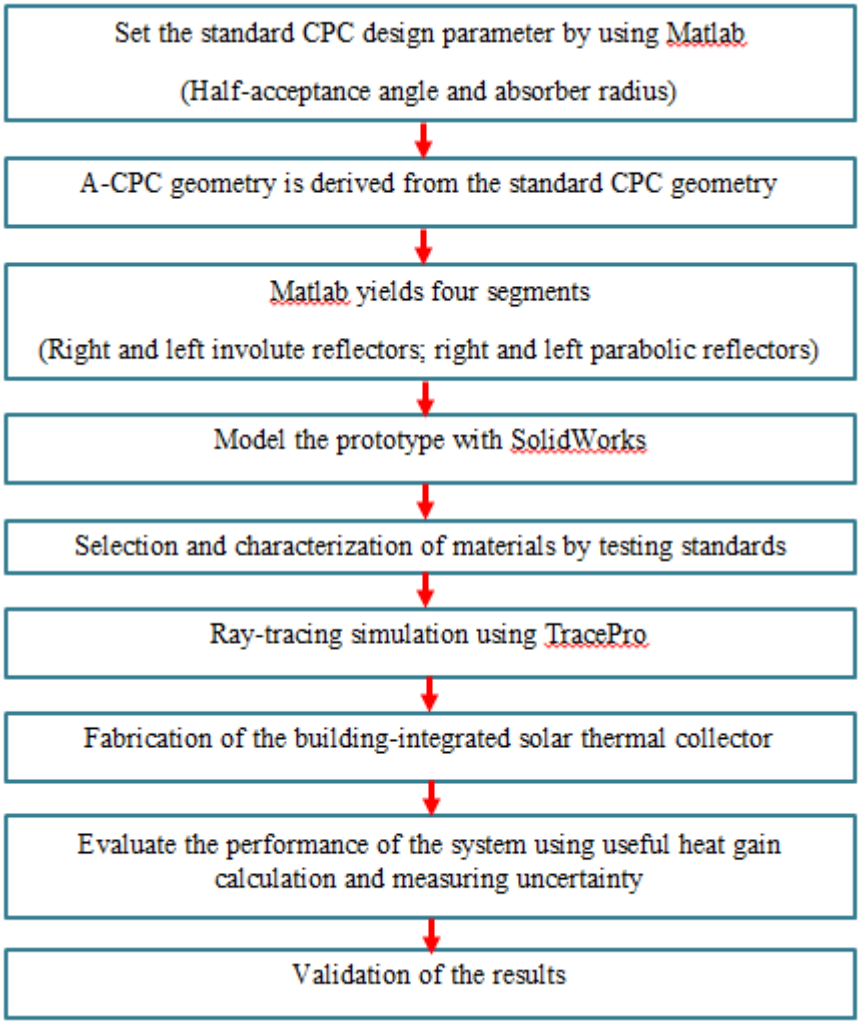

Figure 3-10: Conceptual experimental framework

3.2.1. Design of Building-Integrated A-CPC

a) Determination of design variables and constraints

The optical performance of the A-CPC solar thermal collector is heavily influenced by a variety of parameters, including the half-acceptance angle, concentration ratio, absorber radius and length, gap between the absorber and concentrator, truncation, aperture width, and concentrator reflectivity. The most essential parameter is the half-acceptance angle, which is the maximum angle at which all incoming sun's rays on the collection entry aperture is transferred to the absorber.

The acceptance angle is chosen based on the collector's preferred operating hours, which are at least six hours around midday. In this regard, the acceptance angle is calculated using the solar altitude angles of the summer and winter extreme sun rays. The receiver radius is another important parameter; it is chosen based on the commercially available evacuated tube diameters and the intended application. These two factors were utilized to generate the geometries and determine other dependent parameters like the concentration ratio and collector dimensions like aperture width, height, and height to aperture ratio.

b) Computation of A-CPC Profile

The geometric profile of A-CPC is derived from the standard CPC geometry. The geometric equations for the standard CPC is programmed in Matlab. The parameters are half-acceptance angle and absorber radius. This program yields a conventional structure composed of four segments: right and left involute reflectors, as well as right and left parabolic reflectors, as illustrated in Figure 3-11. The SolidWorks software is then used to develop the 3D model, and the CAD file is then saved and exported in a STEP format.

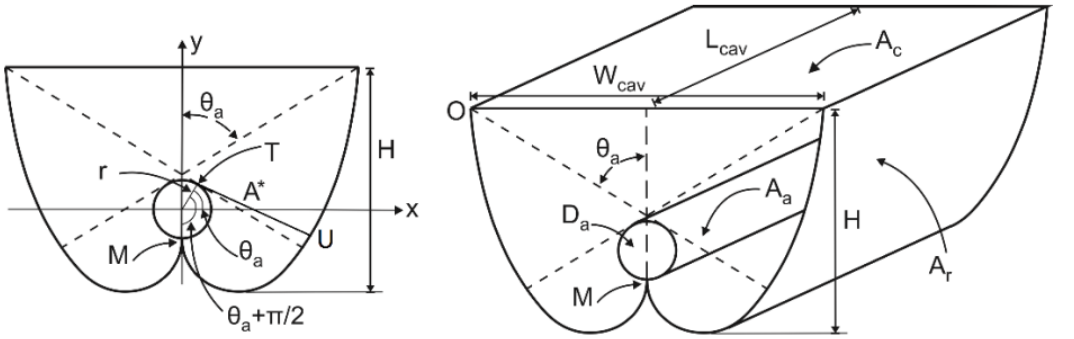

Figure 3-11: Geometry of Standard CPC with a cylindrical absorber (Lara *et al.*, 2021)

Table 3-3: Geometric equations of the CPC with a cylindrical absorber

Geometric concentration (C)	$C = \frac{A_{ap}}{A_r} = \frac{1}{\sin\theta_c}$	3-1
Equations for the parabola segment in the plane (x,y)	$x = r(\sin\theta - M(\theta)\cos\theta)$ $y = -r(\cos\theta + M(\theta)\sin\theta)$ $(\pi/2) + \theta_a \leq \theta \leq (3\pi/2) - \theta_a$	3-2
Line from point U to the tangent of the absorber T is equal to the arc length MT along the absorber circumference	$M(\theta) = \frac{(\pi/2) + \theta_a + \theta - \cos(\theta - \theta_a)}{1 + \sin(\theta - \theta_a)}$	3-3

Equations for the involute segment in the plane (x,y)	$x = r(\sin\theta - \theta\cos\theta)$ $y = r(-\cos t\,\theta - \theta\sin\theta)$ $0 \le \theta \le (\pi/2) + \theta_a$	3-4
CPC reflector area	$A_r = \left[\sum_{i=0}^{\frac{5}{2}\pi} \sqrt{(x^2+y^2)}\right](L_{CPC})$	3-5
Tubular absorber area	$A_a = \pi D_r L_{CPC}$	3-6

Where A_{ap} is the aperture area, A_a the absorber area, A_r is the reflector area, θ the angle between the negative y-axis and the radius to the point of tangency T, r is the radius of the receiver, θ_a is the half-acceptance angle, D_a is the diameter of the absorber, and L_{CPC} is the length of the CPC.

The acceptance angle is computed using the solar altitude angle,

$$\sin\alpha_s = \sin\phi\sin\delta + \cos\phi\cos\delta\cos\omega \qquad 3\text{-}7$$

Where α_s is the sun's altitude angle, ϕ is the latitude (Addis Ababa Institute of Technology, Addis Ababa, Ethiopia, $\phi = 9.040575$), δ is the declination angle, ω is the hour angle, $\omega=0^o$ is the solar noon. To allow the collector to collect sunlight for at least six hours around midday, the hour angle must be deviated 45 degrees before and after the solar noon (15 degrees per hour times). Regarding the declination angle, it can be calculated as follows:

$$\delta = 23.45\sin\left(350\frac{284+n}{365}\right) \qquad 3\text{-}8$$

Where n is the i^{th} day of the year. As a result, the summer and winter extreme sun rays occur when n = 243 and 356, respectively.

3.2.2. Ray-tracing simulation

TracePro, a ray tracing software based on the Monte-Carlo ray-trace technique, is utilized to predict optical assessment for the developed A-CPC collector. TracePro is a robust simulation software that predicts optical efficiency using the Monte-Carlo technique (Tian *et al.*, 2018). The software defines the optical efficiency, which depends on the incidence angle of all incoming radiation. The behavior of the optical rays within the concentrator, the actual concentration ratio, and the flux distribution are all also investigated.

The flowchart in Figure 3-12 depicts the procedures that were followed for executing the TracePro software's ray-tracing simulation for the asymmetrically truncated CPC collector.

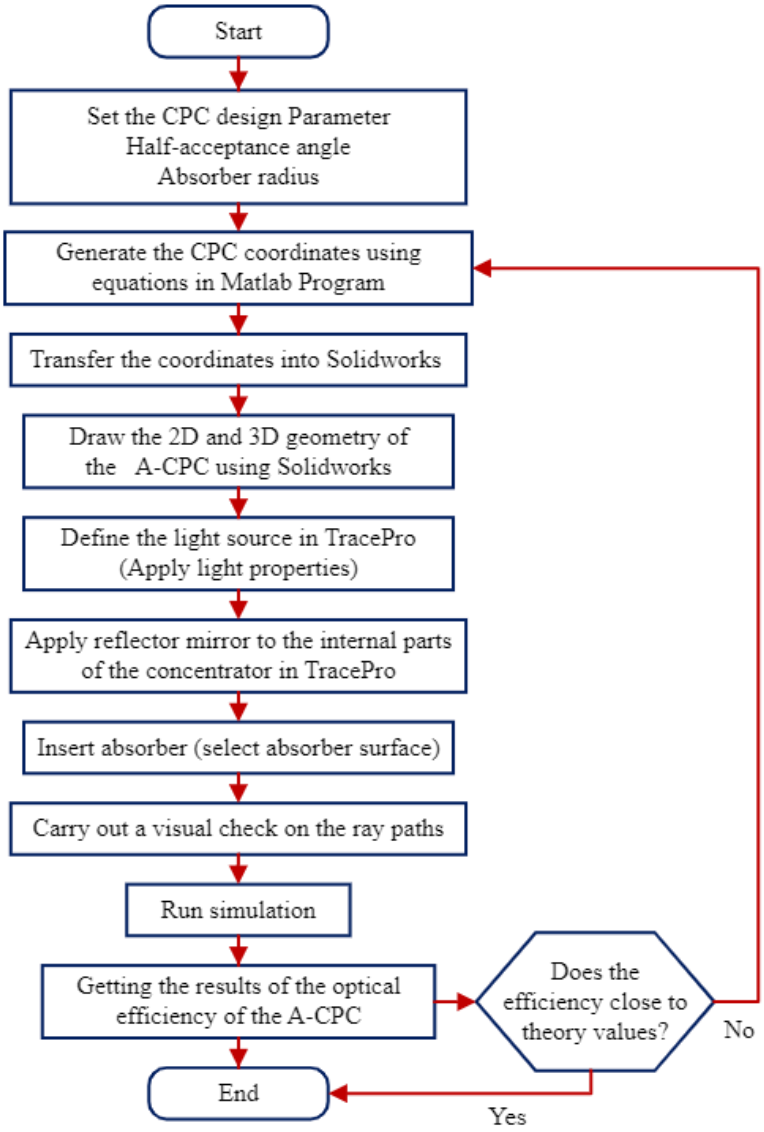

Figure 3-12: The flowchart of the steps of ray-tracing simulation

A number of parameters must be input into TracePro to carry out the simulation. The material type selected for the concentrator body is aluminum and wood. The software provides two types of default reflectors: the perfect mirror and mirror, which have the specular reflectance of 100% and 95%, respectively. In addition, a variety of reflectors from several companies are also available. In this study, the reflector used is the highly reflective film/ reflector Mylar, which is not listed in the software. The reflector Mylar has a reflectivity of 0.95, which indicates that 95% of the incident sun rays will be reflected and 5% of the sun rays absorbed by the reflector Mylar.

Once the material property is identified, the source of light is created. The irradiance intensity has been set to 1000 W/m^2. 10,000 rays in total were used for the simulation, with an angular distribution normal to the surface. The optical properties of the ACPC components are presented in Table 3-4.

Table 3-4: Optical properties of the A-CPC components (Ma *et al.*, 2010)

Component	Material	Reflectivity	Absorptivity	Transmissivity
Reflector	RF015 Reflector Mylar	0.95	0.05	-
Glass envelope	Borosilicate glass	0.075	0.018	0.907
Absorber	Selective coating	0.063	0.93	-

3.3. Testing standards

The Ethiopian Standards Agency adopted the following standards for test procedures, system performance characterization, and specifications for solar thermal systems: ES-ISO 9806: 2015; ES-ISO 9459-1: 2015; 2015; ES-ISO 9459-5: 2015; and ES-ISO 10217: 2015. ES-ISO 9806: 2015 is the most often used standard for evacuated tube collectors.

3.3.1. Test conditions

During the test period, the water temperature at the inlet must be greater than the ambient temperature. If the manufacturer doesn't provide a suggested mass flow rate, then the mass flow rate should be 0.02 kg/s per square meter of solar collector area. The total solar irradiation should not be less than 700 W/m^2 (Ethiopian Standard Agency, 2015).

Table 3-5: Conditions required and deviations for the ES-ISO 9806: 2015 test method

Parameter	Value	Deviation from the mean
Global solar radiation	>700 W/m^2	±50 W/m^2
Mass flow rate	0.02 kg/s m^2	±1%

3.4. Performance Evaluation Method

a) Calculation of useful heat gain

If the mass flow rate, fluid density, specific heat, and inlet and outlet temperatures of the heat transfer fluid are known, it is possible to calculate the useful thermal energy that the collector absorbs.

$$Q_u=\dot{m}C_p(T_2-T_1)=\rho vC_p(T_2-T_1) \quad 3\text{-}11$$

Where: Q_u is the useful heat gain, $\dot{m}$ is the mass flow rate of working fluid (kg/s), C_p is the specific heat (J/kgK), v is the volume flow rate of working fluid (m^3/s), T_2 is the outlet temperature (^oC), and T_1 is the inlet temperature (^oC)

b) Calculation of the collector's actual solar radiation absorption

The actual solar radiation absorption of the collector is determined by the global solar irradiation, aperture area of the collector, and optical efficiency.

$$Q_s=IA_b \qquad 3\text{-}12$$

Where: Q_s is the solar radiation absorption, I is the intensity of solar radiation (W/m^2), and A_b is the absorber area.

c) Calculation of the thermal efficiency

The thermal efficiency of the collector is another important parameter for evaluating the collector's thermal performance. The instantaneous thermal efficiency is expressed as:

$$\eta_{th}=\frac{Q_u}{Q_s}=\frac{\rho v C_p(T_2-T_1)}{IA_b} \qquad 3\text{-}13$$

Where: η_{th} is the instantaneous thermal efficiency.

3.5. Measurement Uncertainty

The overall uncertainty encountered in various measurements is evaluated using the Root Sum Squared (RSS) method (Alammar, 2018).

$$U_o=\pm\sqrt{U_s^2+U_r^2}$$

Where U_o is the overall uncertainity, U_s is the systematic uncertanity, and U_r is the random uncertainity.

According to (Taylor, 1997), the standard uncertainities for dependent varables is given by:

$$\Delta\eta = \pm\eta \times \sqrt{\left(\frac{\Delta T}{T}\right)^2+\left(\frac{\Delta G}{G}\right)^2} \qquad (3.9)$$

CHAPTER FOUR

DESIGN, DEVELOPING AND PERFORMANCE EVALUATION OF A-CPC

This chapter presents the design and development of an Asymmetric Compound Parabolic Concentrator (A-CPC) with a concentric tube heat exchanger. The A-CPC was designed in Solidworks, and the optical analysis was carried out using TracePro software. Sun ray incident on the receiver tube was visualized to identify design faults, ray losses, and reflectance path. Following that, the optical efficiency at various incidence angles is calculated.

4.1. Development of the A-CPC

4.1.1. Design variables

A half-acceptance angle is a key variable, which is the maximum angle at which all incoming rays on the collection entry aperture are transferred to the absorber. Equation 3-7 computations show that the solar altitude angle of the summer's extreme sun rays, which occur at solar noon, is 89.89^o, while the solar altitude angle of the winter's extreme sun rays, which occur three hours before and after solar noon, is 35.33^o. According to this computation, the collector receives all sun rays with solar altitude angles between $\alpha_{s,1}$=35.33^o and $\alpha_{s,2}$=89.89^o. Thus, according to (Rabl, 1976), the acceptance angle of the A CPC is:

$$2\theta_a=\alpha_{s,2}-\alpha_{s,1}=54.56^o$$

The half-acceptance angle is then

$$\theta_a=27.28^o$$

Another important parameter is the receiver radius, which is defined by the diameters of commercially available evacuated glass tubes; in the study, an evacuated glass tube with outer and inner diameters of 58 mm and 47 mm, respectively, was used.

4.1.2. Design of an asymmetric CPC

The receiver radius and half-acceptance angle were used as inputs to a Matlab program that used equations 3-1 to 3-6 to calculate the coordinates of the untruncated CPC. The geometrical properties of the untruncated CPC curve are provided in Table 0-1.

Solidworks is used to build a 2D drawing of the untruncated CPC based on the obtained coordinates. Figure 0-1 depicts the untruncated CPC curve.

Table 0-1: The geometrical properties of the untruncated CPC curve

Parameters	Unit	Value
Half-acceptance angle	o	27.29
Solar altitude acceptance angle	o	35.33 and 89.89
Receiver radius	Mm	23.5
Width of aperture	Mm	322.1
Concentration ratio	-	2.51

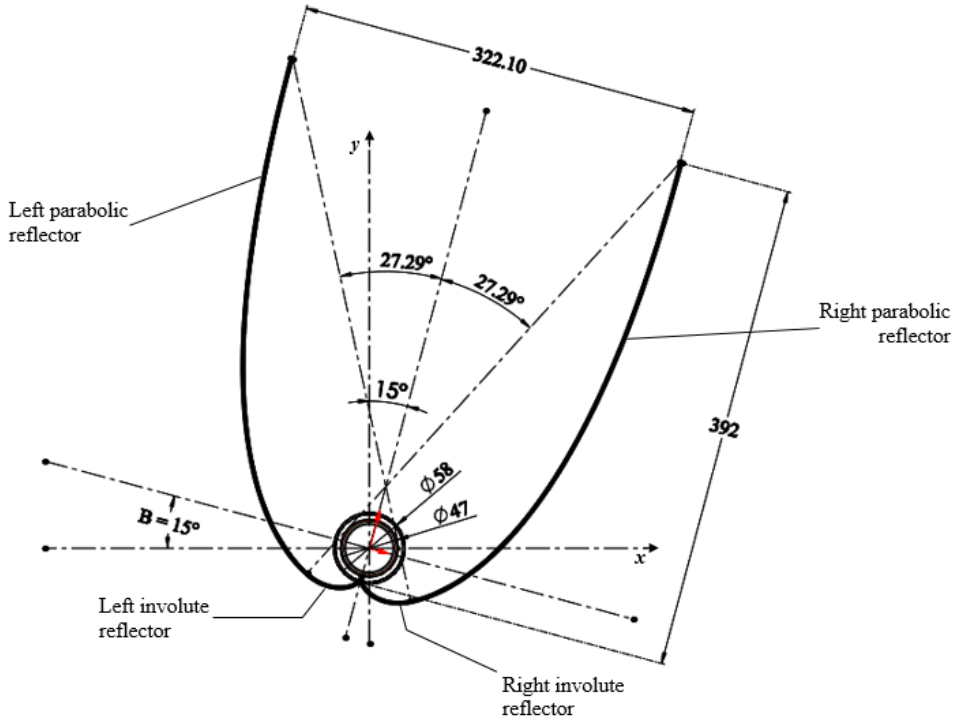

Figure 0-1: The 2D representation of the untruncated CPC

As illustrated in Figure 0-1, the CPC axis is oriented in such a way that maximal solar energy collecting occurs within the acceptance angles. As a rule of thumb, the deflection angle can be considered as the site's latitude. However, in this study a deflection angle of 15 degrees was chosen to prevent the buildup of dirt on the collector.

To prevent the right parabolic reflector from obstructing the evacuated glass tube absorber, the CPC must be truncated. Truncation offers additional benefits including a better concentration ratio and a more aesthetically appealing, compact shape collector that can be adapted for building integration.

Truncation is further recommended to reduce manufacturing and material costs. In Figure 0-2, the line TT indicates the plane of asymmetric truncation.

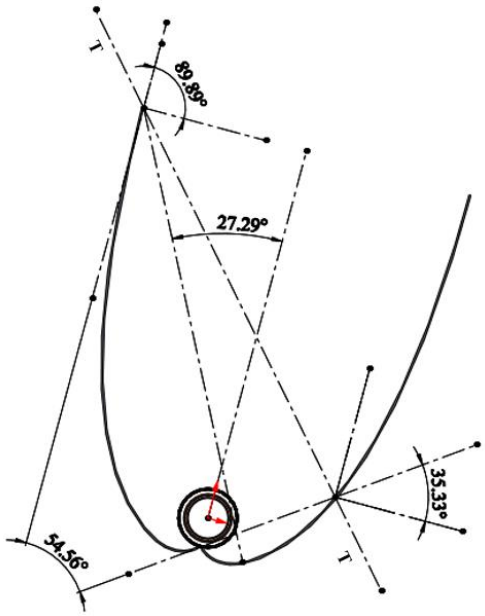

Figure 0-2: The geometry of the CPC that demonstrates asymmetric truncation parameters

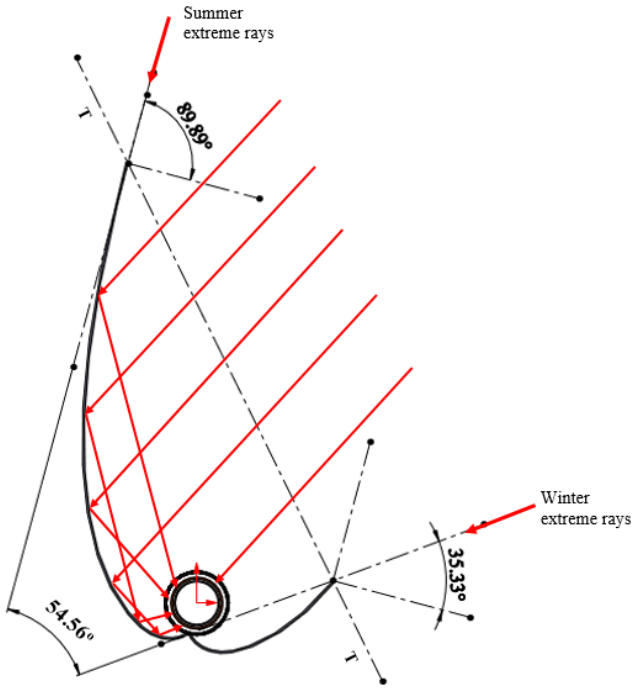

Figure 0-3: The geometry of the A-CPC developed for building integration

The collector, as seen in Figure 0-3, intercepts sun rays with solar altitude angles ranging from 35.33° to 89.89°. The right and left parabolic reflectors are primarily responsible for reflecting the sun's rays within a specific altitude angle. The remaining solar rays are reflected by the right and left involute reflectors, which likewise reflect solar rays that have already been reflected by the parabolic reflectors again to the absorber.

The geometrical concentration ratio of the designed and developed A-CPC can be calculated by dividing the optical aperture area width after truncation by the circumference of the evacuated glass tube absorber (Xuan *et al.*, 2017), as illustrated in Figure 0-3. It can be obtained as follows:

$$C=\frac{\overline{TT}}{2\pi r}$$

where C is the geometric concentration ratio, $\overline{TT}$ is the optical aperture area width, and r is the radius of the reciver.

The optical aperture area width of the A-CPC is 415.34 mm, the acceptance angle is 54.56 degrees, and the concentration ratio is 2.51×. The length is determined by the length of the evacuated glass tube absorber, which is 1800 mm in this case.

4.2. Ray-tracing simulation

The optical efficiency is defined as the ratio of solar power collected at the absorber tube of an evacuated glass tube to the incident solar power on the entry aperture of an A-CPC. The optical efficiency of a A-CPC is calculated by (Akhter *et al.*, 2019):

$$\eta_o=\tau_e\times\tau_d\times\rho^n\times\alpha_i\times f_{ref}\times p$$

where τ_e is the transmittance of the evacuated glass tube's glass envelop, τ_d is the dirt stratification factor of the glass envelop, ρ is the reflectance of the reflective mylar, n is the average number of reflections, α_i is the evacuated glass absorber's absorptance, p is the gap loss coefficient owing to gap width between the glass envelop and the A-CPC, and f_{ref} is multiple reflection coefficients between the glass envelop and inner glass tube.

It is quite challenging to theoretically calculate optical efficiency since it requires complex variables such as the average number of reflections, dirt stratification factor, and gap loss coefficient. Thus, ray tracing software is typically employed to calculate optical efficiency. TracePro, a ray tracing software based on the Monte-Carlo ray-trace technique, is utilized to provide optical assessment for the developed A-CPC collector.

4.2.3. Simulation parameters

To run a ray-tracing simulation in TracePro, several parameters must be provided, including the optical characteristics of the A-CPC reflector surface, the optical characteristics of the evacuated glass tube's glass envelop and absorber, and the surface source, which is the sun's irradiance value, and the solar incidence angle.

Figure 0-4 depicts an A-CPC with a light source. Rays must be emitted from a light source and directed at the concentrator's aperture. The ray source must have the same dimensions as the A-CPC's aperture width and length so that all rays are directed to the aperture. The irradiance intensity has been set to 1000 W/m^2. The sun's mean spectrum is represented by the wavelength of the rays, which is set at 0.5461 m (Amur, 2020). 1,000 rays in total were used for the simulation, with an angular distribution normal to the surface.

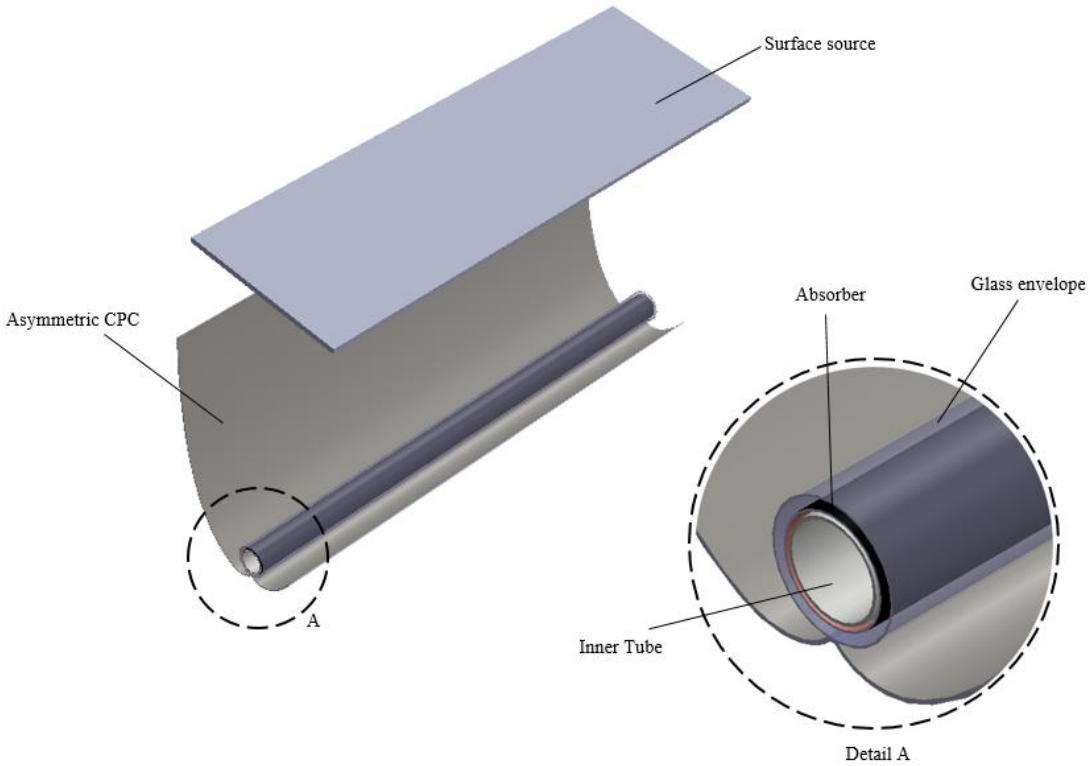

Figure 0-4: The 3D view of A-CPC with identified surfaces

Table 3-4 in the materials and methods chapter shows detailed information regarding the surface properties of A-CPC and material characteristics for evacuated glass tube. The material type used for the A-CPC surface is RF015 reflector Mylar, which has a reflectivity of 0.95, indicating that 95% of incident sun rays are reflected and 5% are absorbed by the reflector Mylar. The evacuated glass tube absorber's absorptivity and the glass envelope's transmissivity coefficients are 0.93 and 0.907, respectively.

4.2.4. Evaluation of the A-CPC optical efficiency

The ray-tracing simulation was carried out between 20.33^{o} and 89.89^{o} with an increment of 7.5^{o} incidence angle to investigate and ensure incident solar radiation reaches the optical aperture of A-CPC. Both the optical efficiency and the flux distribution throughout the collector were calculated and observed. The simulation's output was recorded. The results of the ray tracing are shown in Figures 3.51 to 3.56.

The simulation result at an incident angle of 20.33 degrees is shown in Figure 0-5 (a) and (b). When the incidence angle is 20.33 degrees, incoming solar radiation enters the optical aperture of the A-CPC but is not intercepted by either the parabolic reflectors or the involute mirrors. This demonstrates the effectiveness of the collector's opto-geometric design. The collector, in practice, only collects solar radiation within the range of the predefined solar altitude angle.

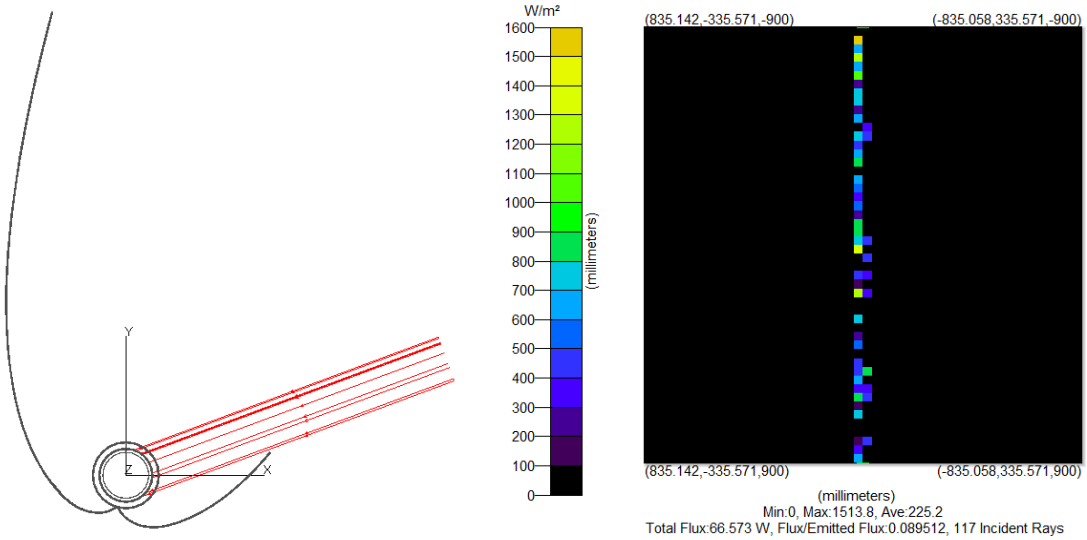

(a) (b)

Figure 0-5: (a) the ray-tracing paths and (b) the irradiance map for absorbed flux at incidence angle of 20.33 degrees

It can be seen from Figure 0-6 that when the incidence angle is 35.33^{o}, the incoming rays can reach the receiver after being intercepted by the right involute mirror. Figure 0-7 shows that when the incidence angle is 50.33 degrees, nearly all the incoming rays reach the receiver after being intercepted by the left and right parabolic reflectors and the right involute mirror. This results in higher optical efficiency.

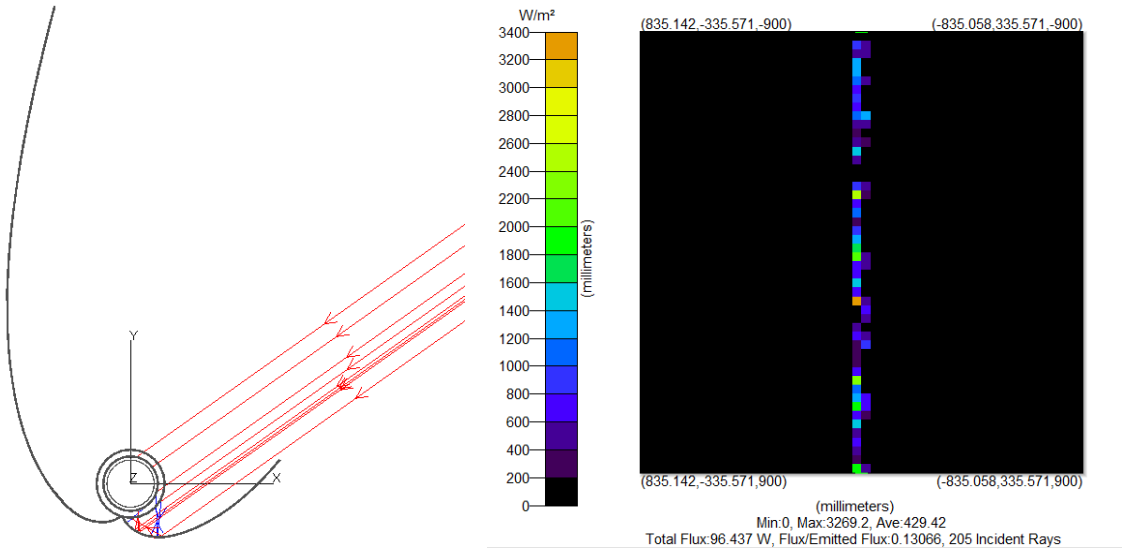

(a) (b)

Figure 0-6: (a) the ray-tracing paths and (b) the irradiance map for absorbed flux at incidence angle of 35.33 degrees

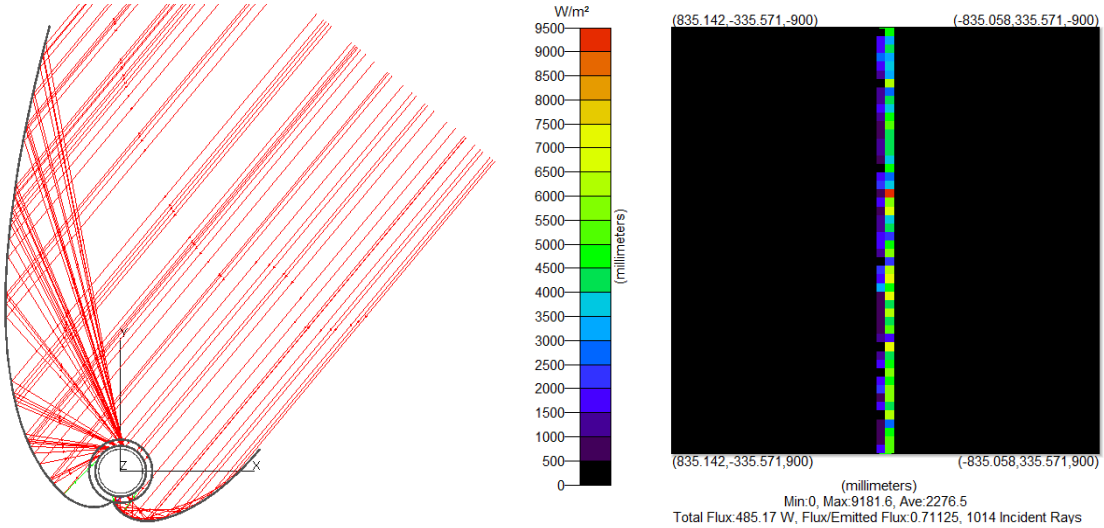

(a) (b)

Figure 0-7: (a) the ray-tracing paths and (b) the irradiance map for absorbed flux at incidence angle of 50.33 degrees

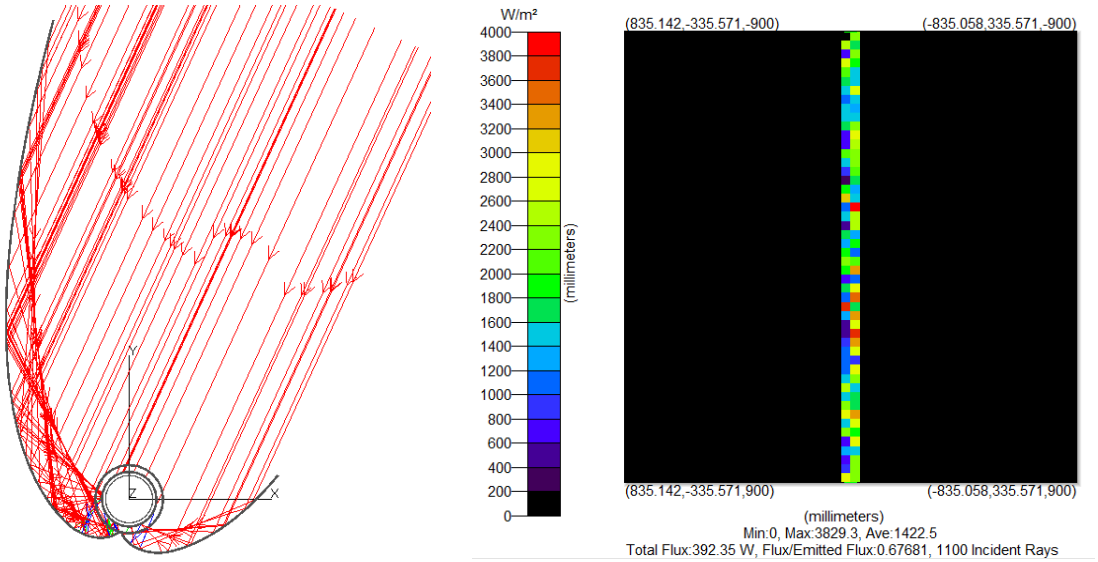

(a) (b)

Figure 0-8: (a) the ray-tracing paths and (b) the irradiance map for absorbed flux at incidence angle of 65.33 degrees

The entering rays were not intercepted by the left parabolic reflector as designed at an incidence angle of 89.89 degrees, as shown in Figure 0-9. This time, the incoming rays are intercepted by the left and right involute mirrors, as well as the right parabolic reflector, before reaching the receiver.

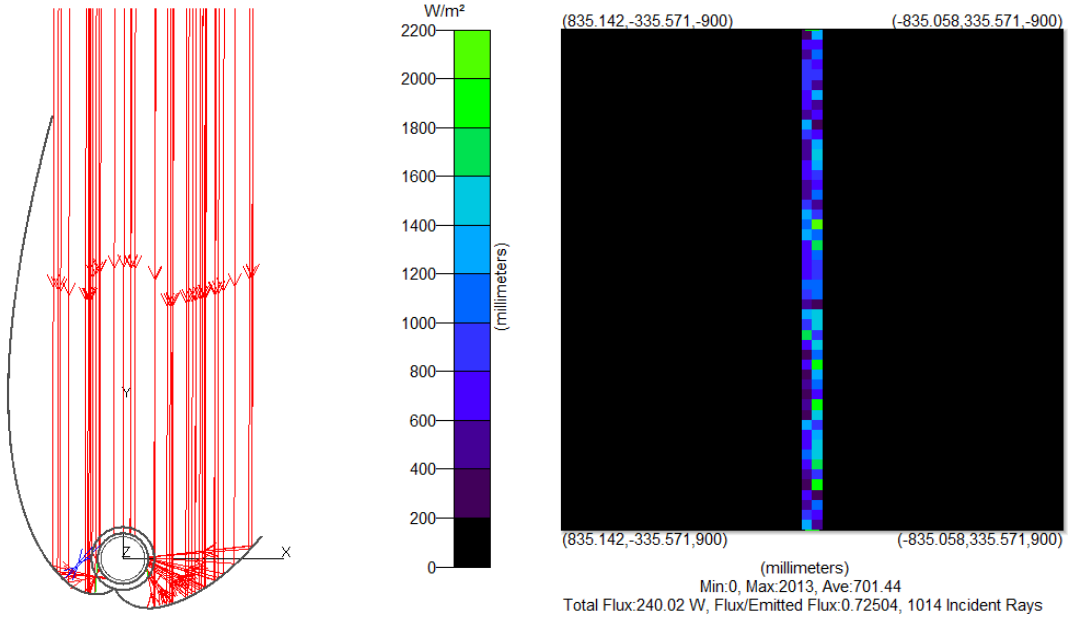

(a) (b)

Figure 0-9: (a) the ray-tracing paths and (b) the irradiance map for absorbed flux at incidence angle of 89.89 degrees

Figure 0-10 depicts the optical efficiency obtained from ray-tracing simulation using TracePro software. As can be seen, when the sun is at its greatest point, the optical efficiency is increased. This is because majority of the sun rays entering the optical aperture fall within the A-CPC's acceptance angles, where they concentrate on the absorber and increase optical efficiency. The results of the ray-tracing simulation also showed that, within the range of the solar altitude angle, the highest optical efficiency is 72.50% and the average optical efficiency is around 57.96%. Based on the results thus far, the ACPC is an ideal concentrator for building integration.

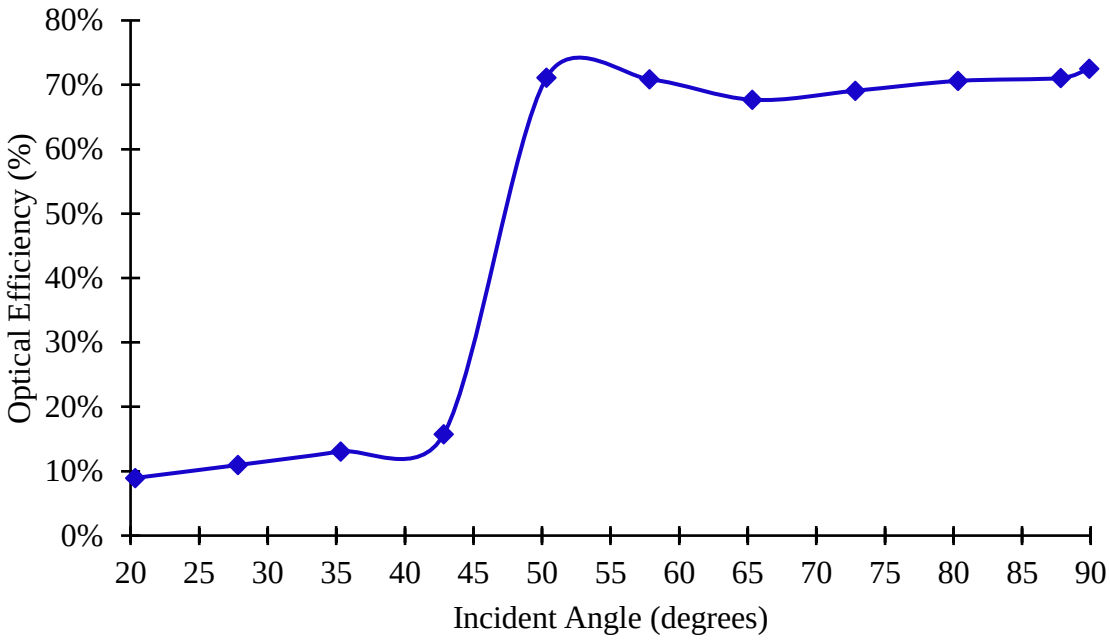

Figure 0-10: Optical efficiency of the A-CPC at different incident angle

CHAPTER FIVE

CONSTRUCTION AND EXPERIMENTAL SETUP

5.1. Construction of Building-Integrated Solar Thermal Collector System

a) Manufacturing of the A-CPC wooden pattern

The A-CPC pattern was cut from a piece of MDF wood considering the resources at hand. First, the concentrator profile was created in SolidWorks and printed on paper. After being cut along the profile's outline, the print was glued to the MDF wood. Following that, the MDF was cut along the marking with an electrical hand jigsaw. Using an electric disk sander, the wooden pattern was then ground to remove any sharp edges. This method produced a precise profile, resulting in an ideal concentrator with minimal reflector surface faults.

(a) (a)

Figure 5-1: Photograph of (a) wooden pattern and (b) gridding the rough edges

b) Manufacturing of the supporting structure

The supporting structure is made of RHS metal frame. Following the construction of the supporting structure, 0.9 mm thick aluminum sheet metal was used to cover the upper portion of the CPC wooden pattern.

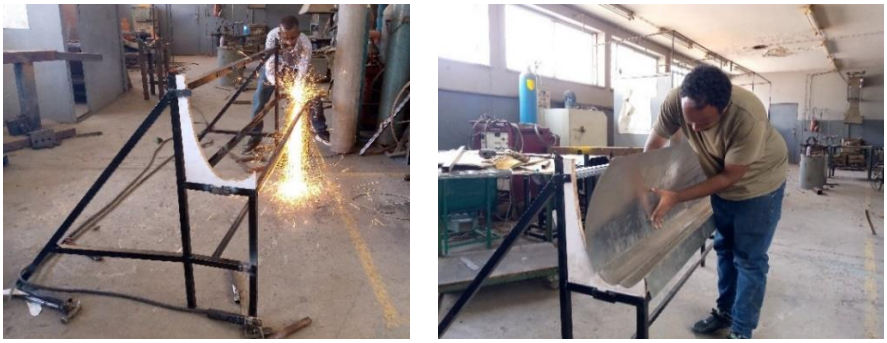

(a) (b)

Figure 5-2: Photographs of fabrication stages of the supporting structure

c) Applying the reflective Mylar

Self-adhesive reflective Mylar, RF015 was applied evenly and floated slightly to enable even distribution without folds and air. The peel-off lining of the reflective Mylar will be taken off prior to the experiment.

(a) (b)

Figure 5-3: Photographs of the reflective Mylar installation process

d) Manufacturing of the concentric tube heat exchanger

Tungsten Inert Gas (TIG) welding is used to manufacture the concentric tube heat exchanger. The inner tube of the annulus has a diameter of 16 mm and a length of 1.6 m, while the outer aluminum has a diameter of 40 mm and a length of 1.7 m. Three radially aligned 2 mm diameter pin spacers are welded to the inner tube to guarantee that the annulus is concentric and to prevent the inner tube from sagging.

(a) (b)

Figure 5-4: Photographs of the coaxial aluminium fluid conduit manufacturing process

5.2. Experiment Test Setup

Figure 5-5 illustrates the experimental test setup for evaluating the performance of the building-integrated solar thermal collector. The test setup is divided into two main parts: the solar thermal collector system and the data acquisition system. The solar thermal collector system is a closed loop system that consists A-CPC, evacuated glass tube, concentric tube heat exchanger, tank, water pump, valves, and other components. The data acquisition system consists primarily of Eppley pyranometer, a CM3 pyranometers, an Extech CFM Thermo-Anemometer, detachable thermocouples, an Eppley electronic-integrator, an NI cDAQ-9172 data logger, and a laptop.

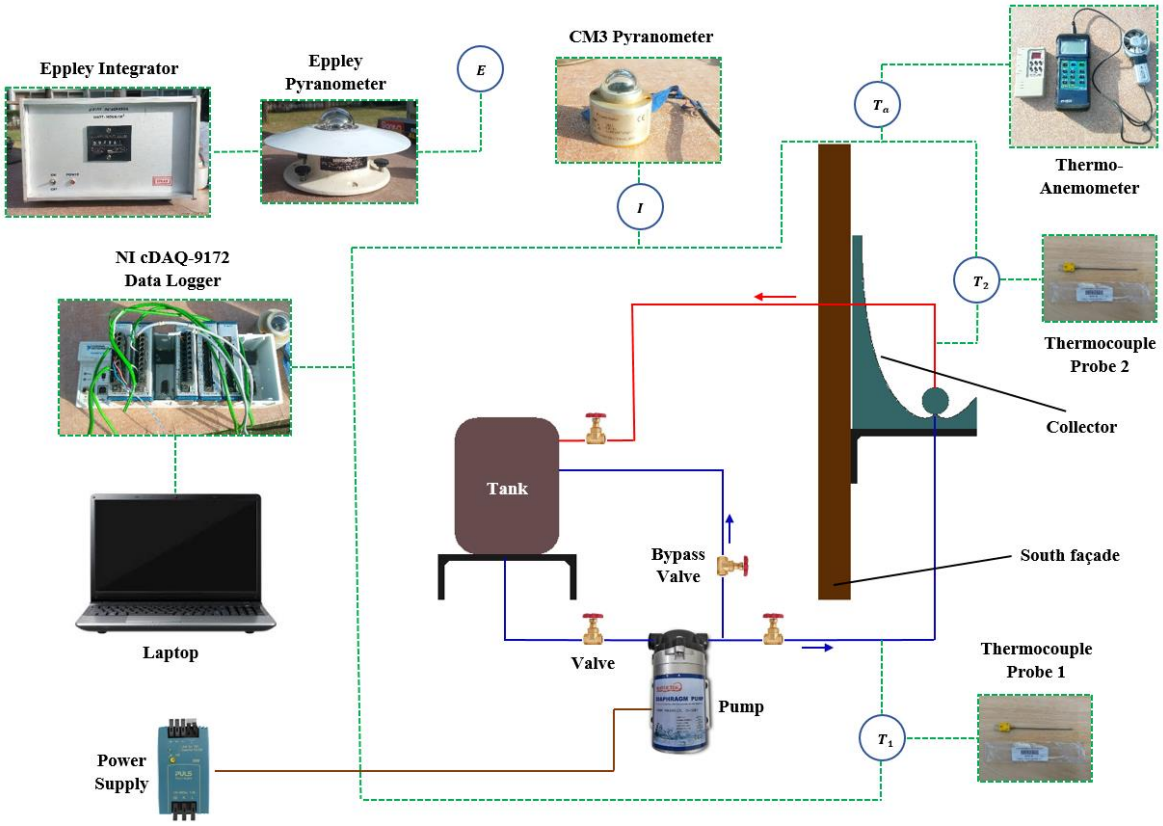

Figure 5-5: The experiment test set-up with measuring instruments

A photograph of the constructed building-integrated solar thermal collector system with data acquisition system is presented in Figure 5-6. The collector was placed at the Addis Ababa Institute of Technology at 9° 2' 26.07" N and 38° 45' 47.5128" E. The collector is positioned vertically and faces south. During the experimental hours, the site was ideal for receiving a large amount of incident solar radiation without shading.

Figure 5-6: Photograph of the actual experimental test setup

Figure 5-7 depicts the data acquisition system that can record and display data from various measurement devices used in the experimental setting.

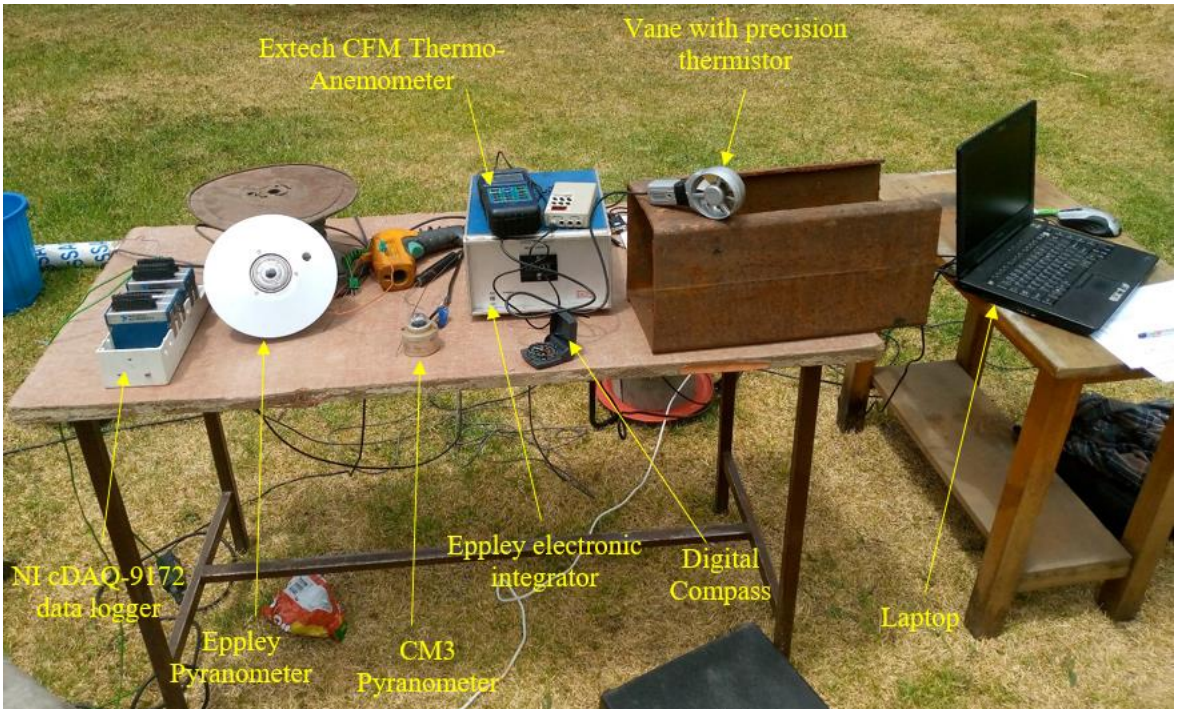

Figure 5-7: Photograph of the actual data acquisition system

Figure 5-8 shows the installation of detachable thermocouples at the inlet and outlet of a concentric tube heat exchanger. The thermocouples wires are linked to the NI cDAQ-9172 data logger.

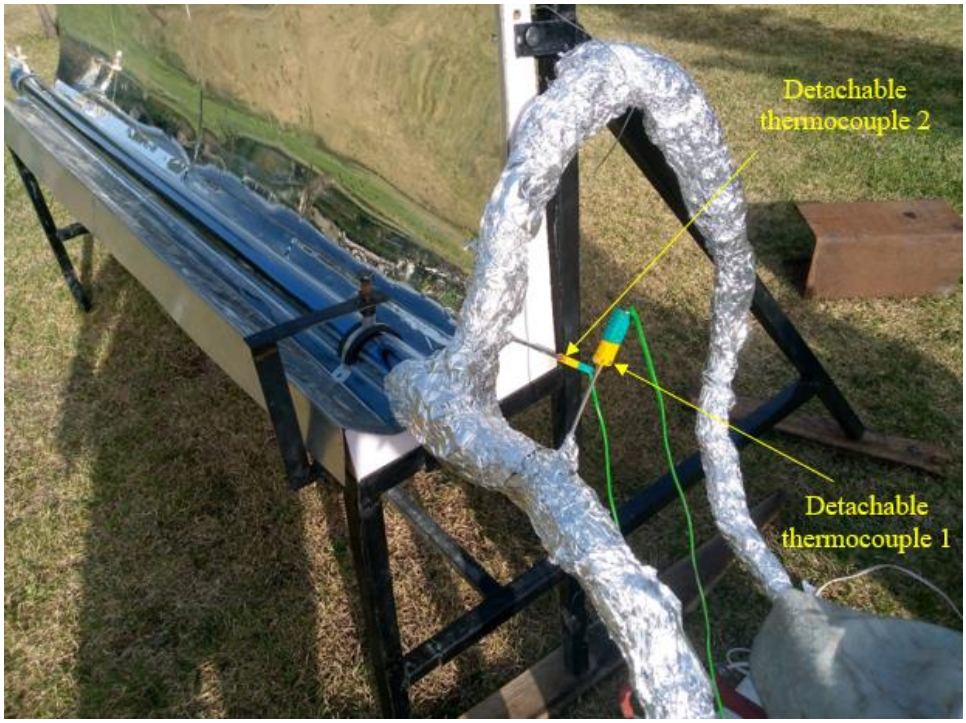

Figure 5-8: Photograph showing location of the thermocouples

CHAPTER SIX
RESULT AND DISCUSSION

In this chapter, the experimental test results of the Asymmetric Compound Parabolic concentrator (A-CPC) evacuated tube collector with concentric tube heat exchanger are presented and discussed. As it has been mentioned in the previous section the collector has been tested using water as working fluid.

Global solar irradiance, working fluid inlet and outlet temperatures, flow rate and ambient temperature were measured since they were considered to evaluate thermal performance. The tests were carried out in 2022 between April and May. However, three representative tests have been chosen to represent the performance of the collector. Their comparative results are discussed in the following sub sections.

6.1. Comparison of Radiation on Horizontal Surface and Aperture Plane

The amount of solar radiation absorbed by the solar collector has a significant impact on its thermal performance. The following section compares solar radiation on a horizontal surface to solar radiation on the aperture plane of a vertically mounted collector.

a) Experiment-1

The first test was carried out on May 19, 2022, and it lasted from 10:16 until 15:31. Figure 6-1 depicts the variation in global solar radiation on the horizontal and aperture plane. Due to frequent cloudy passages and a partially cloudy sky condition, the irradiance on the Aperture plane fluctuated between 169.07 W/m^2 and 768.62 W/m^2.

As it can be seen from the graph, the collector that is mounted vertically receives the least radiation as compared to the horizontal surface. The difference in solar radiation varied throughout the day, with the maximum around noon and the lowest at the end of the experiment. A highest difference of 365 W/m^2 was measured at 12:21.

The result reveals that solar radiation availability on vertically mounted solar collectors is almost less than 30% of the solar radiation incident on the horizontal surface. This shows that conventional solar collectors are unable to satisfy the thermal energy demand of buildings. In this situation, the wall-mounted A-CPC collector can be employed to supply the thermal energy demand of the building even at low solar radiation intensity.

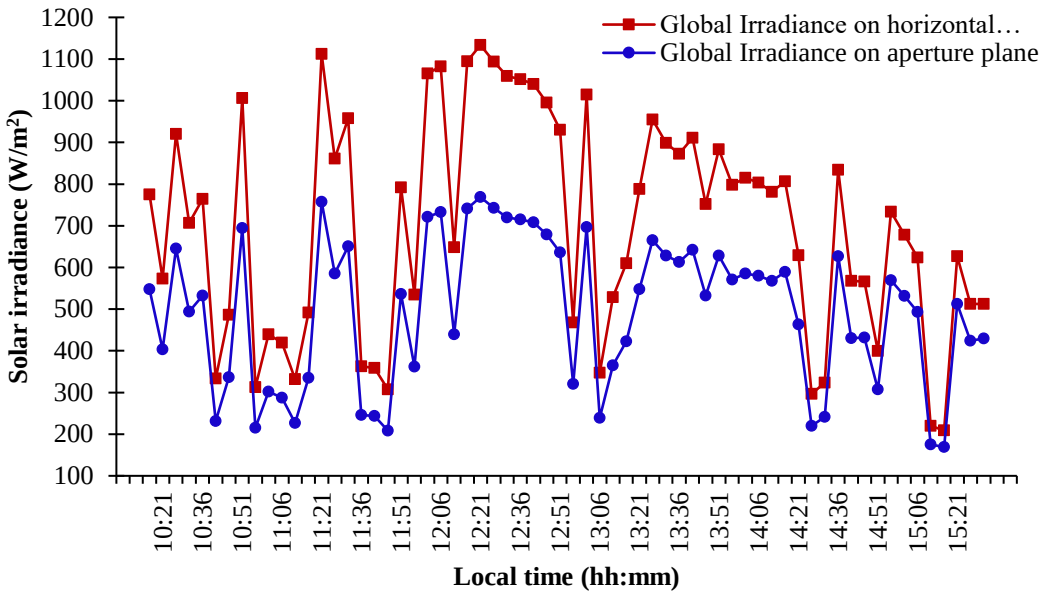

Figure 6-1: Irradiance on horizontal surface and on vertically mounted collector aperture plane, May 19, 2022

b) Experiment-2

The second experiment, which was conducted on May 20, 2022, started at 9:07 and ended at 15:32 in the afternoon. Figure 6-2 depicts the variation in solar radiation during the throughout the experiment period. The sky was almost clear throughout the test; however, there were some cloudy periods, as demonstrated by short-lived drops in solar irradiance. The peak global solar irradiance measured on the Aperture plane was 664.28 W/m^2, while the minimum value is 163.66 W/m^2. As shown in the graph below, at 12:12, a 32% reduction in solar radiation was measured on the aperture plane of a vertically mounted collector when compared to solar radiation incident on a horizontal surface.

a) Experiment-3

The third experimental test was conducted on May 23, 2022, from 9:29 until 15:34. The variation in solar radiation throughout the experiment period is shown Figure 6-3. The global solar irradiance on the Horizontal and Aperture planes at 9:29 was 648.53 W/m^2 and 494.36 W/m^2, respectively. As time passes, the solar irradiance value rises until it reaches a peak of 690.67 W/m^2 on the Aperture plane. At the end of the experiment, the solar irradiance on the Aperture plane was 450.00 W/m^2. In general, the trend of global sun irradiance on the aperture plane increases until 12:19 and then falls as the local time changes. This demonstrated that the third experimental test was carried out under clear sky.

As shown in Figure 6-3, the percentage reduction in solar radiation on the aperture plane of a vertically mounted collector compared to a horizontal surface increases from 9:29 to 12:09, with a peak of 31% at 12:09. As solar radiation drops off, it then starts to decline until it reaches 13.6% at the end of the experiment. The findings showed that without integrating a concentrating collector with the building facades, it would be impossible to meet the thermal energy requirements of a building.

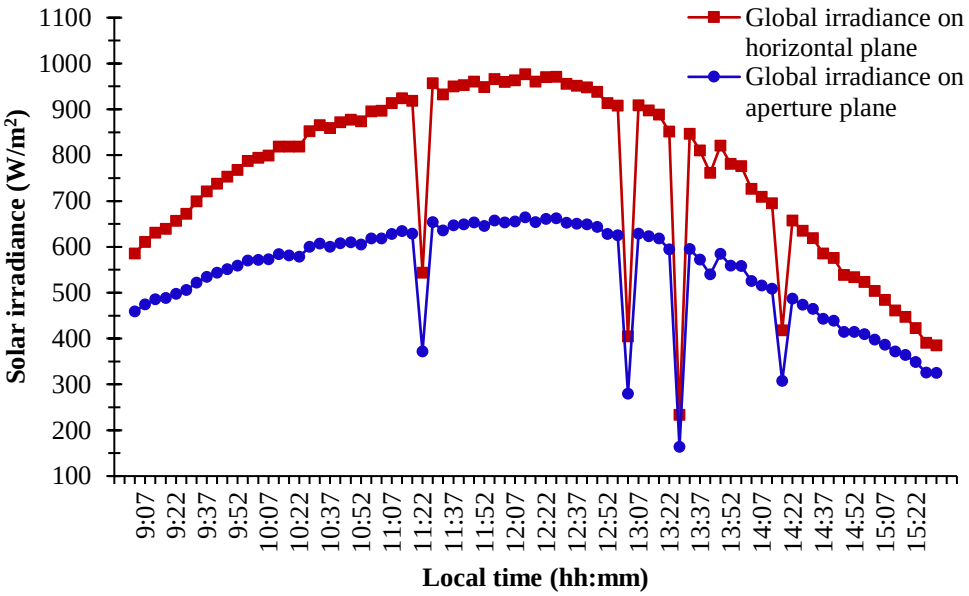

Figure 6-2: Irradiance on horizontal surface and on vertically mounted collector aperture plane, May 20, 2022

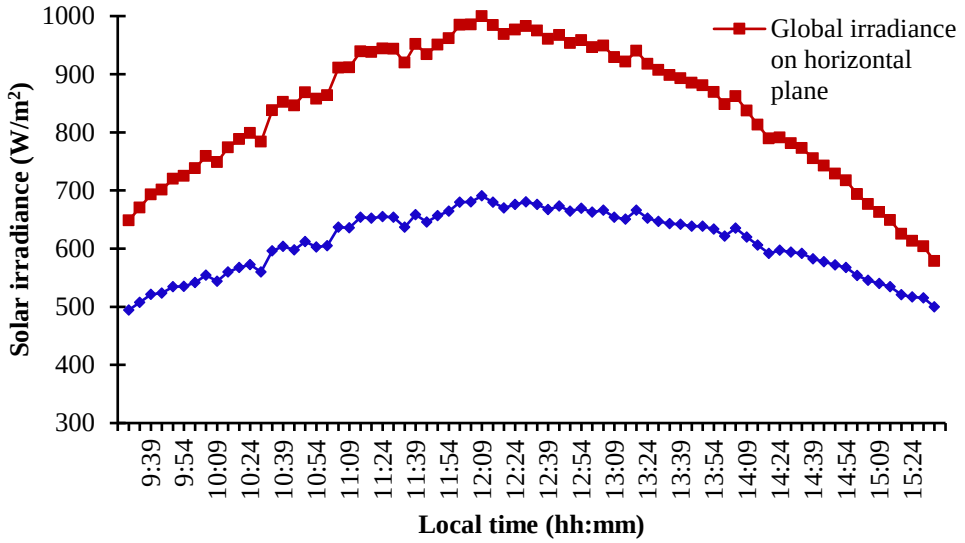

Figure 6-3: Irradiance on horizontal surface and on vertically mounted collector aperture plane, May 23, 2022

In the past, conventional solar collectors were commonly used for building integration, particularly in high-latitude countries where building facades received moderate solar radiation. The experiment result, however, shows that the integration of conventional collectors could not satisfy the thermal demand of buildings in low-latitude countries, where less than 70% of solar radiation is available on building facades. This condition was also mentioned in a study by Cronemberger (Cronemberger, Caamaño-Martín and Sánchez, 2012) that evaluated the solar irradiation potential of building facades at low latitudes. In this sense, a wall-mounted A-CPC collector can be used to meet the thermal energy requirements of the building even when the solar radiation intensity is low.

6.2. Variation in Ambient Temperature with Time

The variation in ambient temperature for May 19, May 20, and May 23 is shown in Figure 6-4. As can be seen in the graph, the ambient temperature is low at the beginning of the experiment in all tests, with values of 29.53°C, 27.07°C, and 27.70°C for May 19, 20, and 23, respectively. On May 19, the outside temperature peaked at 13:36 and was recorded 33.55°C; at 15:11, it reached its lowest point and was recorded 28.69°C. The ambient temperature on the following day ranged from 27.07 to 33.32 degrees Celsius. On May 23, 32.49ºC was found to be the highest ambient temperature measured between 9:29 and 15:59.

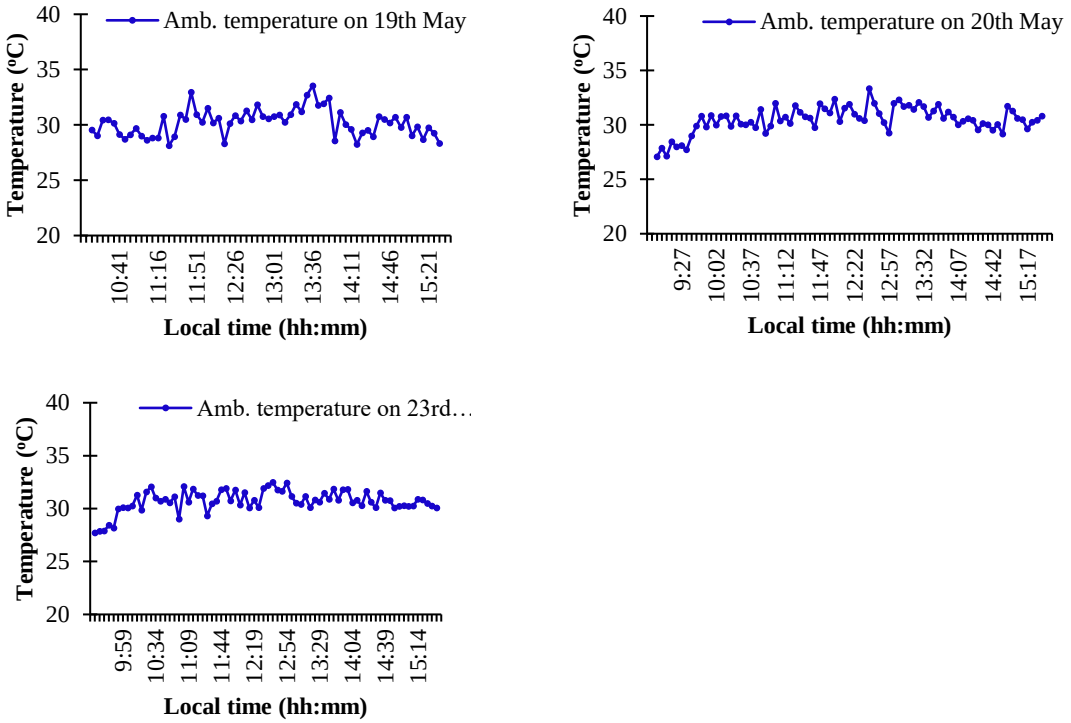

Figure 6-4: Variation in ambient temperature with time

6.3. Variation of Water Temperature with Time

a) Experiment-1

Figure 6-5 depicts the collector's inlet temperature, outlet temperature, and solar irradiance on May 19th 2022. At the beginning of the experiment, the inlet and outlet temperatures gradually rise until 12:11. Then, due to the short-lived clear sky and the resulting intense solar radiation, both begin to rise at a faster rate from 12:16 to 12:51. The outlet temperatures continue to rise, reaching a maximum of 71.30°C at 14:56. After that, it begin to fall until the experiment ends with an outlet temperature of 69.72°C.

Figure 6-6 presents the change in water temperature between inlet and outlet. The partly cloudy weather conditions and the reduced solar irradiance caused the temperature difference to fluctuate significantly. The change in temperature is a function of solar intensity. It was significant from 12:01 to 13:51 and 13:21 to 14:21 because of the less variation of solar radiation due to the relatively clear sky periods. The average temperature difference was 3.27 °C, with the maximum temperature difference occurring at 12:26 and being 5.68 °C.

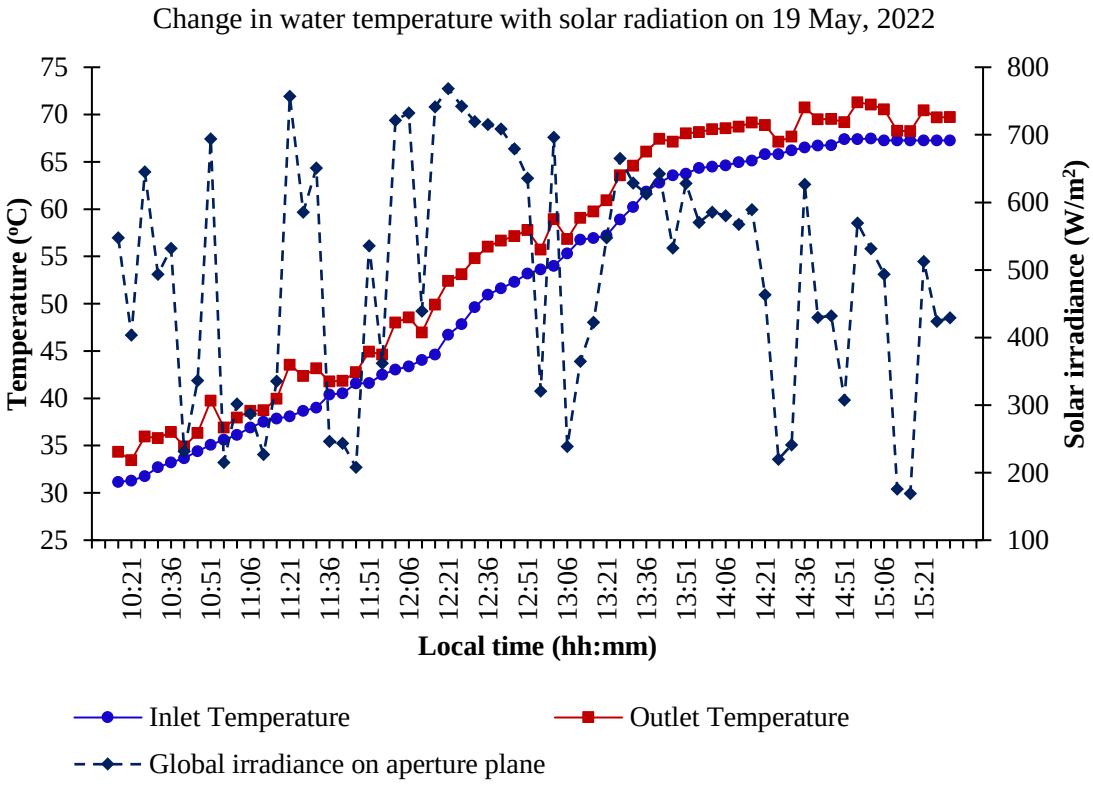

Figure 6-5: Daily water temperature change, May 19th, 2022

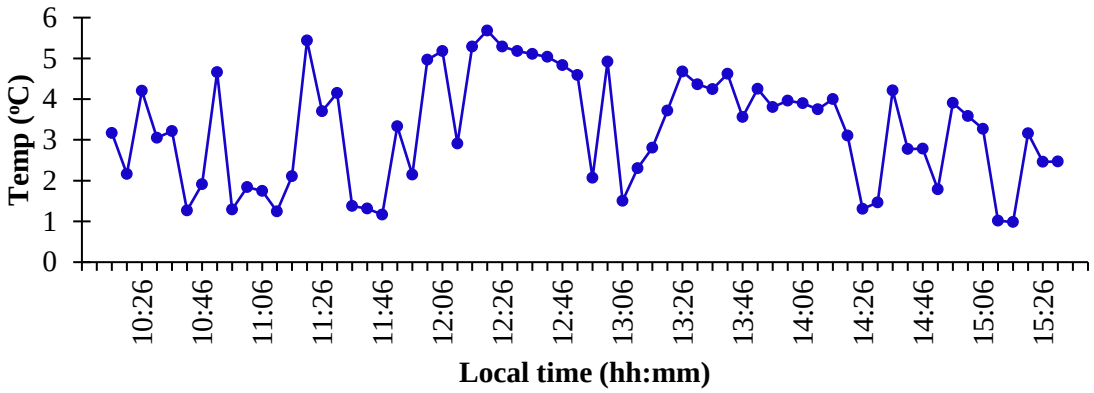

Figure 6-6: Change in water temperature between inlet and outlet, May 19th, 2022

The inlet and outlet temperatures during the experimental test were found to be lower than anticipated for a number of reasons, including (1) heat loss from recirculated high-temperature water passing through the bypass valve, (2) heat loss from the 1.0 mm air gap between the evacuated tube and the outer surface of the coaxial tube, and (3) heat loss from an insulated valve and 1.5 cm thick insulated pipes exposed to the atmosphere.

b) Experiment-2

Figure 6-7 shows the recorded results for experiment two conducted on May 20th, 2022. The outlet temperature ranged from 30.43°C to 78.21°C, whereas the inlet temperature ranged from 28.07°C to 74.79°C. At 14:02, the outlet water reaches its highest possible temperature, 78.21°C, with solar radiation of 524.82 W/m^2 on the aperture plane. The graph shows that the water's outlet temperature increase up until 13:47, then slightly decreased as the sun's irradiance decreased. It has also been demonstrated that solar irradiance directly influences the temperature difference between the inlet and outlet.

The temperature difference between the water's inlet and outlet is shown in Figure 6-8. On this day, the sky is relatively clear, so there is less fluctuation in the temperature. The graph also shows that temperature change is directly proportional to solar intensity. The maximum temperature difference was found to be 4.61°C at 12:12, with the average temperature difference being 3.52°C.

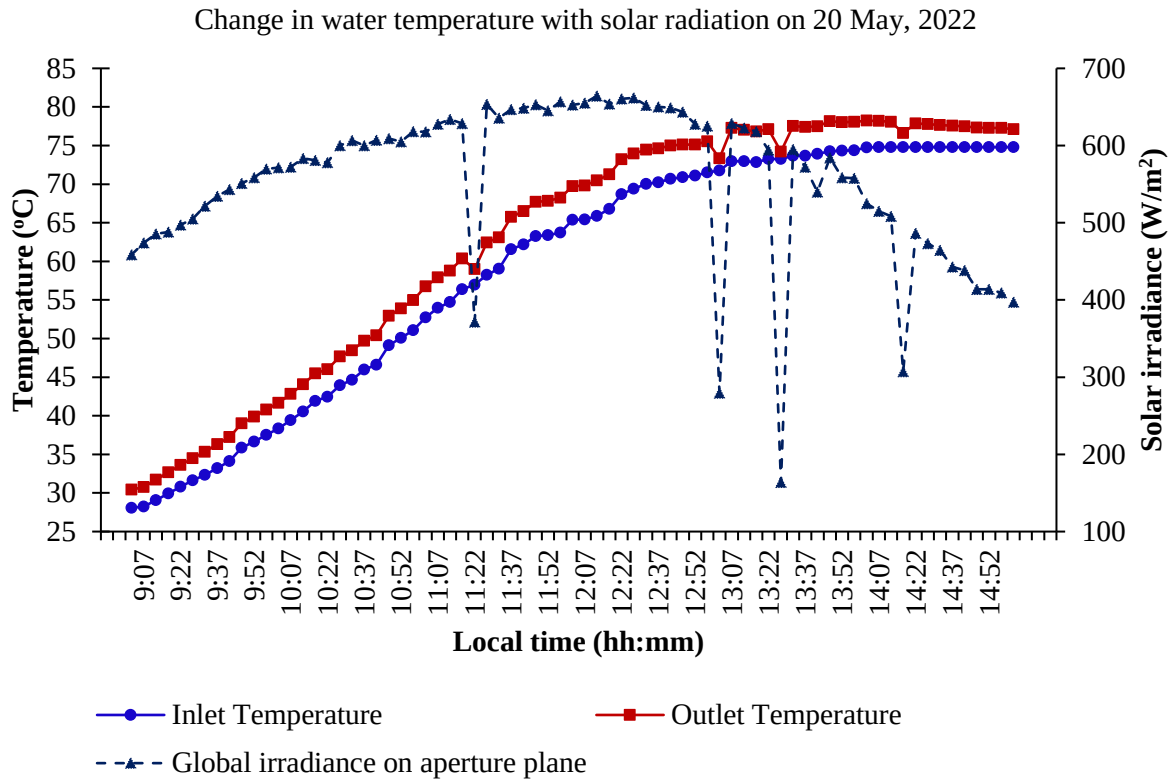

Figure 6-7: Daily water temperature change, May 20th, 2022

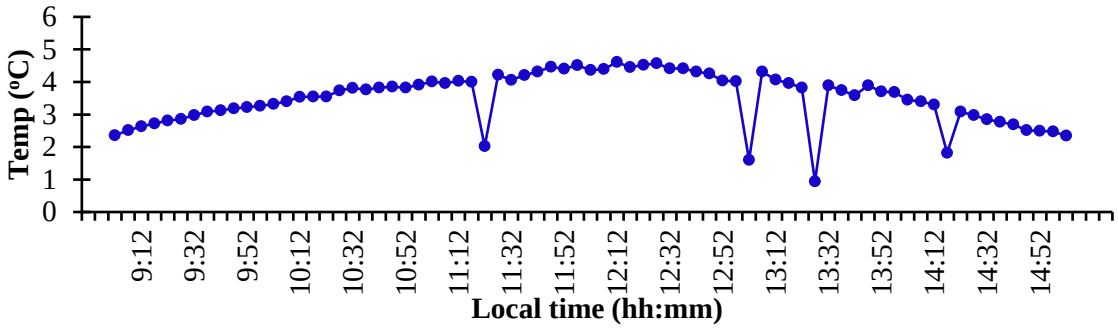

Figure 6-8: Change in water temperature between inlet and outlet, May 20th, 2022

c) Experiment-3

Figure 6-9 shows the experimental findings from the third experiment, which was carried out on May 23, 2022, on a sunny and clear sky day with maximum solar radiation estimated to be around 690.67 W/m^2 on the aperture plane. On that day, the outlet temperature nearly increased linearly with time from the start of the experiment to 12:14. And continued to rise, reaching a maximum temperature of 80.04ºC about 14:44. Following that, the temperature increase started to decline as a result of (1) a drop in solar radiation after noon time and (2) an increase in the system's heat loss as a result of the rising water temperature.

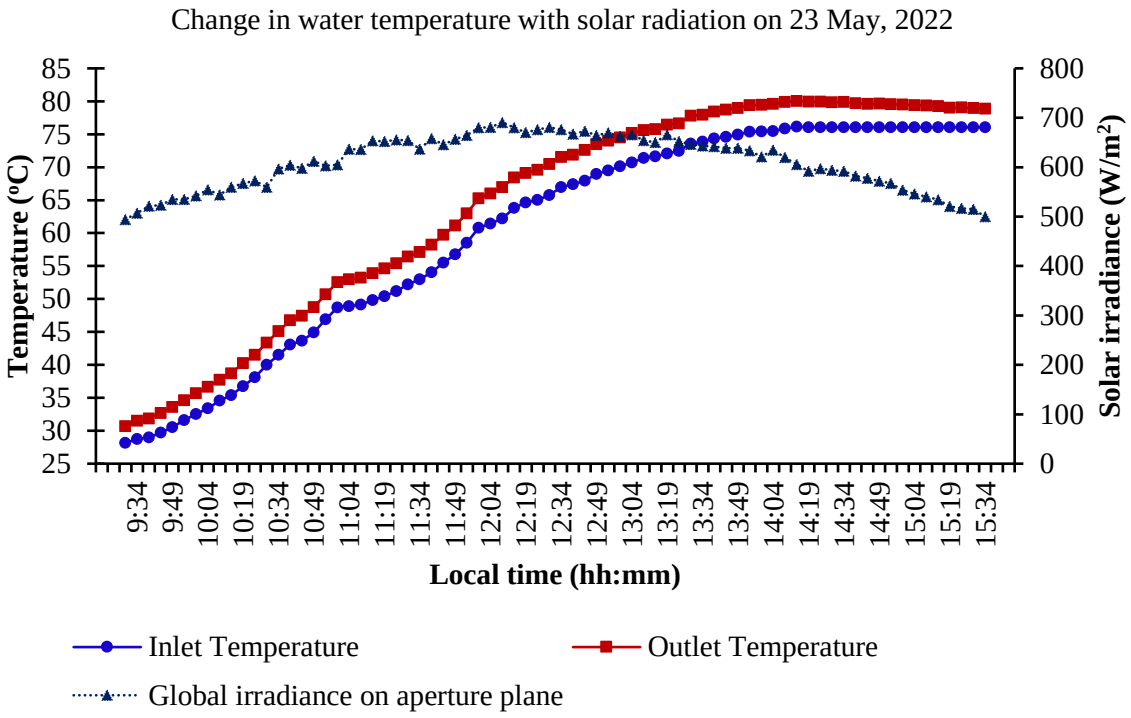

Figure 6-9: Daily water temperature change, May 23rd, 2022

In contrast to the earlier tests, the temperature difference during the third test was comparatively constant from start to finish, as shown in Figure 6-10. This is because there were no clouds passing that day, and the sky was clear. The graph also indicates a direct relationship between the rate of temperature change and the intensity of solar radiation. Furthermore, it can be seen that the temperature continued to rise until noon as solar radiation increased.

The change in temperature peaked at 4.73°C at the time the solar radiation reached its highest level of that day. After reaching its peak, the temperature started to decrease along with the solar radiation intensity. The average temperature difference was approximately 3.86°C.

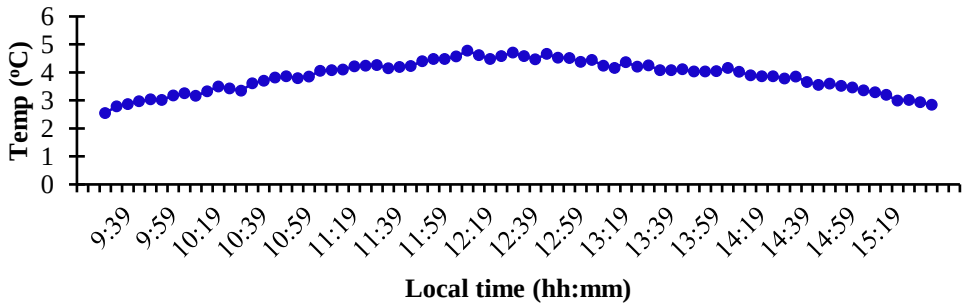

Figure 6-10: Change in water temperature between inlet and outlet, May 23rd, 2022

In their preliminary investigation on the photo-thermal performance of building integrated solar collectors, (Chenggang and Fei, 2020) reported a maximum temperature of 77^{o}C, Another study by (Zheng et al., 2015) demonstrated that the highest temperature of the tracking compound curved surface concentrator under a clear sky was 80°C.

6.4. Variation of Useful Energy Gain with Time

Figure 6-11 demonstrates the variation in instantaneous useful gained heat with respect to time for experiments carried out on May 19, May 20, and May 23. Due to the frequent periods of cloudy weather, the heat gain in the first experiment was highly variable. It varied from 58.39 W to 337.38 W. The average gained heat was measured to be 194.11 W. The second experiment was conducted under a relatively clear sky. Due to the relatively low solar radiation at the start of the experiment at 9:02, the useful heat gained was only 139.91 W. However, as time passes, it increased with an increase in solar radiation, reaching a peak value of 273.53 W at 12:12, demonstrating that the amount of energy collected is influenced by the rate of solar radiation. The heat gained varied smoothly on the third day due to less variance in solar radiance. The range of the useful heat gained was 151.49 W to 283.29 W. The average heat gained was found to be 229.18 W.

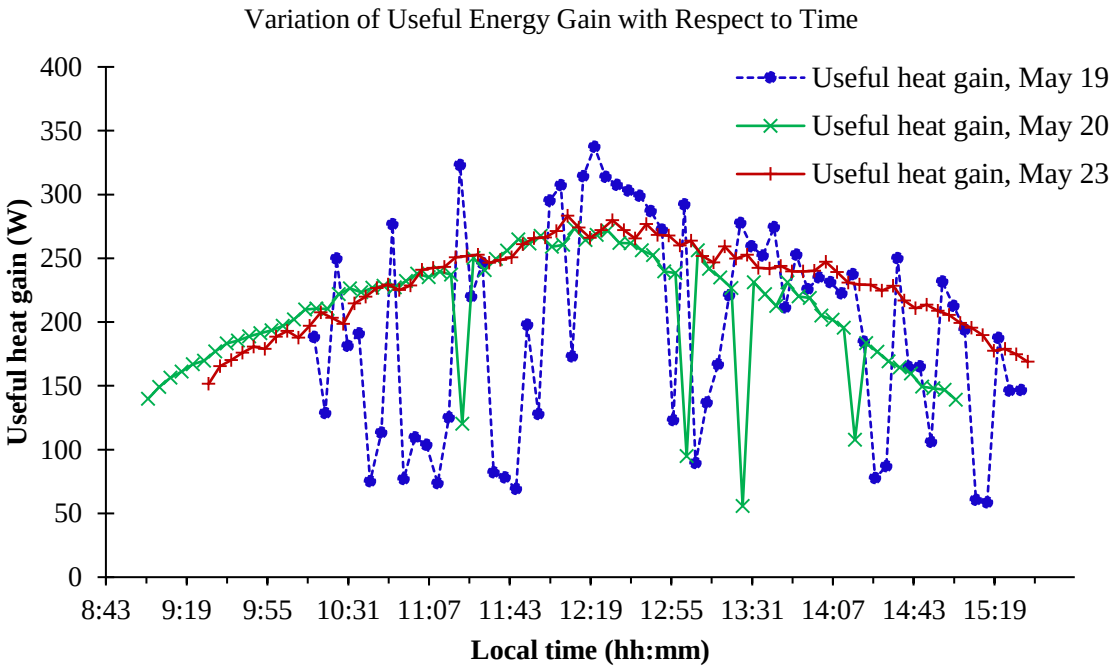

Figure 6-11: Variation of useful energy gain with to time

6.5. Variation of Thermal efficiency with Time

The thermal efficiency of the collector during the first, second and third tests is illustrated in Figure 6-12. During the first test, the maximum instantaneous thermal efficiency and average thermal efficiency of the collector was around 58.71% and 51.20%, respectively. Due to the partially cloudy weather that day, the collectors' thermal efficiency varied significantly throughout the test period. It was evident during the second test on the following day that the instantaneous thermal efficiency fluctuated less because of the relatively clear weather. The maximum instantaneous thermal efficiency was found to be around 58.32%, while the average thermal efficiency value was calculated to be around 52.86%. The third test, conducted on May 23, revealed that the collector's instantaneous thermal efficiency and average thermal efficiencies are 58.27% and 53.03%, respectively.

It can be seen that the thermal efficiency for all tests periods was maximum at midday, while it was lower at the beginning and at the end. This could be due to two factors: (1) the collector was designed to intercept solar rays with an altitude angle ranging from 35.33^{o} to 89.89^{o}, causing the collector to receive less solar radiation at the beginning and end; and (2) the collector's orientation and the effect of wind load.

This phenomenon has also been observed in other studies (Harmim *et al.*, 2013, 2019; Kashiide, Akisawa and Enoki, 2015; Zheng *et al.*, 2015; Deng and Chen, 2020; Mboup, Nakayama and Akisawa, 2020).

Based on the examination of the degree of uncertainty mentioned in the methodology section, the uncertainties of temperature difference and sun irradiation are 2.0% and 10.0%, respectively. Taking systematic and random error into account, the maximum uncertainty of instantaneous thermal efficiency is 6.0%, 5.95%, and 5.94% for experiments 1, 2, and 3, respectively.

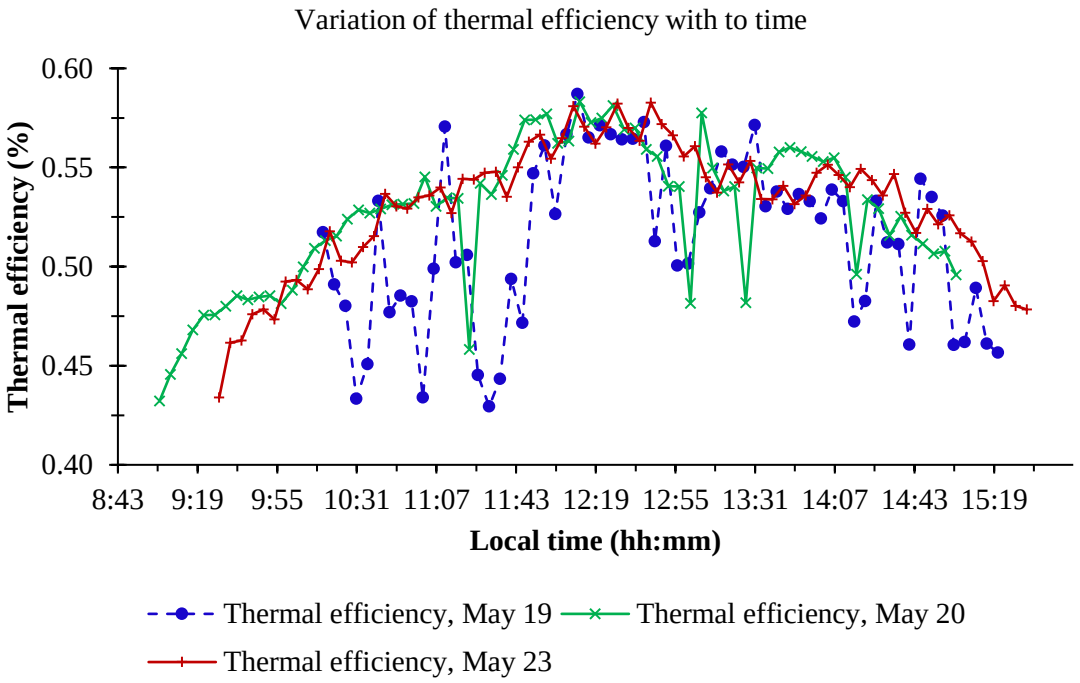

Figure 6-12: Variation of thermal efficiency with to time

The reported tests on the thermal performance of building-integrated collectors are summarized in Figure 6-13.

Figure 6-13: Summary of results on thermal efficiency of the collector

No	Parameter	Unit	This work			(Chenggang and Fei, 2020)
			Test 1	Test 2	Test 3	
1	Volume flow rate	litter/hr	51	51	51	45
3	Maximum solar radiation on horizontal plane	W/m^2	1134	976	1000	850
4	Minimum solar radiation on horizontal plane	W/m^2	209	233	579	300
5	Starting temperature of water	^oC	31	28	28	30
6	Highest water temperature	^oC	71	78	80	77
7	Thermal efficiency	%	51.2	52.86	53.03	51.4

CHAPTER SEVEN
CONCLUSION AND RECOMMENDATION

7.1. Conclusion

An Asymmetric Compound Parabolic concentrator (A-CPC), which was made of an evacuated tube collector with concentric tube heat exchanger, has been designed and tested. The A-CPC's geometric profile allows it to be integrated into a building façade in low-latitude nations such as Ethiopia. It has the ability to capture solar radiation for at least six hours a day in order to meet the huge thermal energy demands of buildings.

TracePro, raytracing software, was utilized to predict the optical efficiency of the collector by simulating its optical performance at various sun altitude angles. The results showed that, within the range of the solar altitude angle, the highest optical efficiency is about 73% and the average optical efficiency is around 58%. This result indicated that the developed A-CPC is capable of capturing solar energy incidents on the building walls.

From the experimental result, it was found that the maximum attained water temperature for experiment-1, experiment-2, and experiment-3 was 71^{o}C, 78^{o}C, and 80^{o}C, respectively. The average water temperature difference between inlet and outlet of the collector is 3.27 ^{o}C, 3.52 ^{o}C, and 3.86^{o}C for flow rate of 51 liter per hour in experiment-1, experiment-2, and experiment-3, respectively. The experimental results also revealed that during the first experiment, the collector's instantaneous thermal efficiency peaked at about 58.71% and averaged out at about 51.20%. In the second experiment, the maximum and average thermal efficiencies were 58.32% and 52.86%, respectively. The thermal efficiency and average thermal efficiencies in the third experiment is found to be 58.27% and 53.03%, respectively.

In conclusion, the optical evaluation and experiments demonstrated that the building-integrated Asymmetric Compound Parabolic Concentrator (A-CPC) solar thermal collector has a high efficiency and is ideal for harvesting solar radiation available on building facades. Moreover, the results demonstrated that, in contrast to popular belief, the integration of solar collectors on building façade at low latitude countries is viable and should be taken into consideration.

7.2. Recommendation

Based on the observations made during this study, the following recommendations are given to improve the system's performance.

1. In this study, the air gap between the exterior of the concentric tube and the evacuated tube is neglected. Even if the air gap is too small, it can have a significant impact on the rate of heat transfer and the efficiency of the collector in low ambient temperature and windy environments. Therefore, the impacts of air gaps should be studied.
2. The collector's performance has not been tested on a real building façade. Therefore, further studies are needed to evaluate the thermal performance of the collector and its impact on building heating and cooling.
3. In this analysis, only the south walls of the structure are taken into consideration. However, a significant amount of solar energy can be harnessed from the east, west, and north walls of buildings. This would make it possible to meet the building's year-round demand for thermal energy. As a result, more research is required to assess the possibilities of harvesting solar radiation from the east, west, and north walls of buildings.
4. The investigation of the collector's thermal characteristics is limited to experimental investigation. For the experimental result to be validated, the thermal behavior of the collector should be simulated.

REFERENCE

Abdullahi, B. *et al.* (2017) 'Effects of Acceptance angle and Receiver radius on the Optical Performance of Compound Parabolic Collector', *Nigerian Journal of Solar Energy*, 28, pp. 1–9.

Akhter, J. *et al.* (2019) 'Optical performance analysis of single flow through and concentric tube receiver coupled with a modified CPC collector under different configurations', *Energies*, 12(21). Available at: https://doi.org/10.3390/en12214147.

Alammar, A.A.G. (2018) *Enhancing thermal performance of heat pipe based solar thermal collector*.

Aldegheri, F. *et al.* (2014) 'Building integrated low concentration solar system for a self-sustainable Mediterranean villa: The Astonyshine house', *Energy and Buildings*, 77, pp. 355–363. Available at: https://doi.org/10.1016/j.enbuild.2014.03.058.

Amur, M. (2020) *Design, Fabrication and Characterisation of Cross Compound Parabolic Concentrators for Solar Power Generation*. Cardiff University.

Brito, M.C. *et al.* (2017) 'The importance of facades for the solar PV potential of a Mediterranean city using LiDAR data', *Renewable Energy*, 111, pp. 85–94. Available at: https://doi.org/10.1016/j.renene.2017.03.085.

Buker, M.S. and Riffat, S.B. (2015) 'Building integrated solar thermal collectors - A review', *Renewable and Sustainable Energy Reviews*. Elsevier, pp. 327–346. Available at: https://doi.org/10.1016/j.rser.2015.06.009.

Buonomano, A. *et al.* (2019) 'Building-façade integrated solar thermal collectors: Energy-economic performance and indoor comfort simulation model of a water based prototype for heating, cooling, and DHW production', *Renewable Energy*, pp. 20–36. Available at: https://doi.org/10.1016/j.renene.2018.01.059.

Chemisana, D. (2011) 'Building integrated concentrating photovoltaics: A review', *Renewable and Sustainable Energy Reviews*, 15(1), pp. 603–611. Available at: https://doi.org/10.1016/j.rser.2010.07.017.

Chenggang, D. and Fei, C. (2020) 'Preliminary investigation on photo-thermal performance of a novel embedded building integrated solar evacuated tube collector with compound parabolic concentrator', *Energy*, 202, p. 117706.

Chow, T.T., He, W. and Ji, J. (2007) 'An experimental study of fac photovoltaic / water-heating system', 27, pp. 37–45. Available at: https://doi.org/10.1016/j.applthermaleng.2006.05.015.

Cronemberger, J., Caamaño-Martín, E. and Sánchez, S.V. (2012) 'Assessing the solar irradiation potential for solar photovoltaic applications in buildings at low latitudes - Making the case for Brazil', *Energy and Buildings*, 55, pp. 264–272. Available at: https://doi.org/10.1016/j.enbuild.2012.08.044.

Deng, C. and Chen, F. (2020) 'Preliminary investigation on photo-thermal performance of a novel embedded building integrated solar evacuated tube collector with compound parabolic concentrator', *Energy*, 202, p. 117706. Available at: https://doi.org/10.1016/j.energy.2020.117706.

Desthieux, G. *et al.* (2018) 'Solar energy potential assessment on rooftops and facades in large built environments based on lidar data, image processing, and cloud computing. Methodological background, application, and validation in geneva (solar cadaster)', *Frontiers in Built Environment*, 4(March). Available at: https://doi.org/10.3389/fbuil.2018.00014.

Dineshkumar, P. (2016) *Computer Aided Design, Analysis and Performance Investigations on a Solar Compound Parabolic Concentrator*. Rai University.

Ethiopian Standard Agency (2015) *ES ISO 9806 : 2015 : Solar Energy - Solar Thermal Collectors - Test Methods*. Available at: https://www.iso.org/standard/17186.html.

Frattolillo, A. *et al.* (2020) 'Potential for building Façade-integrated solar thermal collectors in a highly urbanized context', *Energies*, 13(21), pp. 1–18. Available at: https://doi.org/10.3390/en13215801.

Gagliano, A., Aneli, S. and Nocera, F. (2019) 'Analysis of the performance of a building solar thermal facade (BSTF)for domestic hot water production', *Renewable Energy*, 142, pp. 511–526. Available at: https://doi.org/10.1016/j.renene.2019.04.102.

Gao, Y. *et al.* (2013) 'Effects of thermal mass and flow rate on forced-circulation solar hot-water system: Comparison of water-in-glass and U-pipe evacuated-tube solar collectors', *Solar Energy*, 98(PC), pp. 290–301. Available at: https://doi.org/10.1016/j.solener.2013.10.014.

Glembin, J., Rockendorf, G. and Scheuren, J. (2010) 'Internal thermal coupling in direct-flow coaxial vacuum tube collectors', *Solar Energy*, 84(7), pp. 1137–1146. Available at: https://doi.org/10.1016/j.solener.2010.03.018.

Harmim, A. *et al.* (2013) 'Design and experimental testing of an innovative building-integrated box type solar cooker', *Solar Energy*, 98(PC), pp. 422–433. Available at: https://doi.org/10.1016/j.solener.2013.09.019.

Harmim, A. *et al.* (2019) 'Simulation and experimentation of an integrated collector storage solar water heater designed for integration into building facade', *Energy*, 166, pp. 59–71. Available at: https://doi.org/10.1016/j.energy.2018.10.069.

He, G. *et al.* (2015) 'Promotion of building-integrated solar water heaters in urbanized areas in China: Experience, potential, and recommendations', *Renewable and Sustainable Energy Reviews*, 42, pp. 643–656. Available at: https://doi.org/10.1016/j.rser.2014.10.044.

Huang, J. *et al.* (2019) 'Solar water heating systems applied to highrise buildings-lessons from experiences in China', *Energies*, 12(16). Available at: https://doi.org/10.3390/en12163078.

Ilija Nasov (2015) 'Solar Energy in Architecture: the Case of Facade Collectors', *International Journal of Engineering Research and Technology (IJERT)*, 4(1), pp. 1–4. Available at: www.ijert.org.

IRENA (2020) *Renewable Energy Policies in a Time of Transition: Heating and Cooling, Energy Policy*.

Isa, M.M., Rahman, A. and Goh, H.H. (2015) 'Design Optimisation of Compound Parabolic Concentrator (CPC) for Improved Performance', *International Journal of Electrical, Computer, Energetic, Electronic and Communication Engineering*, 9(5), pp. 2–4.

Ji, J. *et al.* (2010) 'Modelling and validation of a building-integrated dual-function solar collector', *Journal of Power and Energy*, 225, pp. 259–269. Available at: https://doi.org/10.1177/2041296710394243.

Ji, X. *et al.* (2015) 'Effect of Installation of Solar Collector on Performance of Balcony Split Type Solar Water Heaters', *International Journal of Photoenergy*, 2015. Available at: http://dx.doi.org/10.1155/2015/865041.

Jiang, C. *et al.* (2020) 'A review of the compound parabolic concentrator (CPC) with a tubular absorber', *Energies*, 13(3). Available at: https://doi.org/10.3390/en13030695.

Kashiide, R., Akisawa, A. and Enoki, K. (2015) 'Performance of wall-mounted non-tracking solar thermal collector with a parabolic mirror for concentration', in *ISES Solar World Congress 2015, Conference Proceedings*, pp. 880–889. Available at: https://doi.org/10.18086/swc.2015.10.02.

Kayali, H. and Dr. Halil Alibaba, A.P. (2017) 'Comparison of Different Solar Thermal Energy Collectors and Their Integration Possibilities in Architecture', *Sustainability in Environment*, 2(1), p. 36. Available at: https://doi.org/10.22158/se.v2n1p36.

Kumar, A., Said, Z. and Bellos, E. (2021) 'An up-to-date review on evacuated tube solar collectors', *Journal of Thermal Analysis and Calorimetry*, 145(6), pp. 2873–2889. Available at: https://doi.org/10.1007/s10973-020-09953-9.

Lamnatou, C. *et al.* (2016) 'Building-integrated solar thermal systems based on vacuum-tube technology : Critical factors focusing on life-cycle environmental pro fi le', *Renewable and Sustainable Energy Reviews*, 65, pp. 1199–1215. Available at: https://doi.org/10.1016/j.rser.2016.07.030.

Lara, F. *et al.* (2021) 'Design, optimization and comparative study of a solar CPC with a fully illuminated tubular receiver and a fin inverted V-shaped receiver', *Applied Thermal Engineering*, 184, p. 116141. Available at: https://doi.org/10.1016/j.applthermaleng.2020.116141.

Lee, K.H. *et al.* (2014) 'Annual measured performance of building-integrated solar energy systems in demonstration low-energy solar house', *Journal of Renewable and Sustainable Energy*, 6(4), pp. 1–15. Available at: https://doi.org/10.1063/1.4893467.

Li, G., Xuan, Q., Akram, M W, *et al.* (2020) 'Building integrated solar concentrating systems : A review', *Applied Energy*, 260(November 2019), p. 114288. Available at: https://doi.org/10.1016/j.apenergy.2019.114288.

Li, G., Xuan, Q., Akram, M. W., *et al.* (2020) 'Building integrated solar concentrating systems: A review', *Applied Energy*, 260(September 2019), p. 114288. Available at: https://doi.org/10.1016/j.apenergy.2019.114288.

Li, R., Dai, Y. and Wang, R. (2015) 'Experimental investigation and simulation analysis of

the thermal performance of a balcony wall integrated solar water heating unit', *Renewable Energy*, 75, pp. 115–122. Available at: https://doi.org/10.1016/j.renene.2014.09.023.

Li, X. *et al.* (2013) 'Comparative study on two novel intermediate temperature CPC solar collectors with the U-shape evacuated tubular absorber', *Solar Energy*, 93, pp. 220–234. Available at: https://doi.org/10.1016/j.solener.2013.04.002.

Ma, L. *et al.* (2010) 'Thermal performance analysis of the glass evacuated tube solar collector with U-tube', *Building and Environment*, 45(9), pp. 1959–1967. Available at: https://doi.org/10.1016/j.buildenv.2010.01.015.

Maurer, C., Cappel, C. and Kuhn, T.E. (2017) 'Progress in building-integrated solar thermal systems', *Solar Energy*, 154, pp. 158–186. Available at: https://doi.org/10.1016/j.solener.2017.05.065.

Mboup, A., Nakayama, M. and Akisawa, A. (2020) 'Design and performance evaluation of a wall mounted solar concentrating collector', *Thermal Science and Engineering Progress*, 19(January), p. 100593. Available at: https://doi.org/10.1016/j.tsep.2020.100593.

Muhammad-Sukki, F. *et al.* (2014) 'Mirror symmetrical dielectric totally internally reflecting concentrator for building integrated photovoltaic systems', *Applied Energy*, 113, pp. 32–40. Available at: https://doi.org/10.1016/j.apenergy.2013.07.010.

Naik, B.K. and Muthukumar, P. (2019) 'Performance assessment of evacuated U-tube solar collector: a numerical study', *indian Academy of Sciences*, 44(1). Available at: https://doi.org/10.1007/s12046-018-0974-z.

Nie, X. *et al.* (2017) 'Experimental study on thermal performance of U-type evacuated glass tubular solar collector with low inlet temperature', *Solar Energy*, 150, pp. 192–201. Available at: https://doi.org/10.1016/j.solener.2017.04.030.

Ong, K.S., Tong, W.L. and Choong, J.K. (2016) 'Performance of U-tube solar water heater with vertical and inclined panels', *International Journal of Low-Carbon Technologies*, 11(2), pp. 248–253. Available at: https://doi.org/10.1093/ijlct/ctt063.

PEA (2021) *Assessment for the Implementation of Solar Water Heaters to Hotels, Hospitals and Other Commercial Buildings in Addis Ababa*.

Pradhan, D., Mitra, D. and Neogi, S. (2016) 'Thermal Performance of a Heat Pipe Embedded Evacuated Tube Collector in a Compound Parabolic Concentrator', *Energy Procedia*, 90(December 2015), pp. 217–226. Available at: https://doi.org/10.1016/j.egypro.2016.11.188.

Rabl, A. (1976) 'Optical and thermal properties of compound parabolic concentrators', *Solar Energy*, 18(6), pp. 497–511. Available at: https://doi.org/10.1016/0038-092X(76)90069-4.

Rabl, A., Goodman, N.B. and Winston, R. (1979) 'Practical design considerations for CPC solar collectors', *Solar Energy*, 22(4), pp. 373–381. Available at: https://doi.org/10.1016/0038-092X(79)90192-0.

Redweik, P., Catita, C. and Brito, M. (2013) 'Solar energy potential on roofs and facades in an urban landscape', *Solar Energy*, 97, pp. 332–341. Available at: https://doi.org/10.1016/j.solener.2013.08.036.

Taylor, J.R. (1997) *An Introduction to Error Analysis: The Study of Uncertainties in Physical Measurements*.

Tian, M. *et al.* (2018) 'A review on the recent research progress in the compound parabolic concentrator (CPC) for solar energy applications', *Renewable and Sustainable Energy Reviews*, 82(June 2016), pp. 1272–1296. Available at: https://doi.org/10.1016/j.rser.2017.09.050.

Ulavi, T., Hebrink, T. and Davidson, J.H. (2014) 'Analysis of a hybrid solar window for building integration', *Energy Procedia*, 57, pp. 1941–1950. Available at: https://doi.org/10.1016/j.egypro.2014.10.058.

Ustaoglu, A. *et al.* (2018) 'Truncation effects in an evacuated compound parabolic and involute concentrator with experimental and analytical investigations', *Applied Thermal Engineering*, 138, pp. 433–445. Available at: https://doi.org/10.1016/j.applthermaleng.2018.04.062.

Visa, I., Moldovan, M. and Duta, A. (2020) 'Experimental performance assessment of vertically installed solar thermal collectors', *Journal of Sustainable Development of Energy, Water and Environment Systems*, 8(4), pp. 692–700. Available at: https://doi.org/10.13044/j.sdewes.d7.0287.

Wang, J. *et al.* (2016) 'Optical analysis of solar collector with new V-shaped CPC', *Solar Energy*, 135, pp. 780–785. Available at: https://doi.org/10.1016/j.solener.2016.06.019.

Wang, P.Y., Li, S.F. and Liu, Z.H. (2015) 'Collecting performance of an evacuated tubular solar high-temperature air heater with concentric tube heat exchanger', *Energy Conversion and Management*, 106, pp. 1166–1173. Available at: https://doi.org/10.1016/j.enconman.2015.10.058.

Xuan, Q. *et al.* (2017) 'Optimization design and performance analysis of a novel asymmetric compound parabolic concentrator with rotation angle for building application', *Solar Energy*, 158(October), pp. 808–818. Available at: https://doi.org/10.1016/j.solener.2017.10.029.

Yang, M. *et al.* (2020) 'Optical and thermal performance analysis of a micro parabolic trough collector for building integration', *Applied Energy*, 260(May 2019), p. 114234. Available at: https://doi.org/10.1016/j.apenergy.2019.114234.

Yang, Y. *et al.* (2013) 'A building integrated solar collector: All-ceramic solar collector', *Energy and Buildings*, 62, pp. 15–17. Available at: https://doi.org/10.1016/j.enbuild.2013.03.002.

Zhang, X. *et al.* (2015) 'Building Integrated Solar Thermal (BIST) Technologies and Their Fundamentals of Renewable Energy and Applications', *Journal of Fundamentals of Renewable Energy and Applications*, 5(November), pp. 0–21. Available at: https://doi.org/10.4172/20904541.1000182.

Zheng, H. *et al.* (2015) 'Design and Testing of a Shell-Encapsulated Solar Collector with the Compound Surface Concentrators', *International Journal of Photoenergy*, 2015. Available at: https://doi.org/10.1155/2015/130187.

APPENDIX

Appendix A: Matlab code for computation of CPC geometry (Adopted from Mathworks)

```
%% Plots a Involute part of CPC
%hold off
syms teta;
r=58;
r1 = 58;  %radius of reciver
r2 = 47;
% Involute area M <= |teta| <= tetaA + pi/2
% From trigenometry - tetaM = cos-1(r/(r+lg))
tetaA = degtorad(30);   % Half-acceptance angle
pInvTheta = r*teta; % Pteta = distance along tangential line from absorber to curve
% Reflector part tetaA + pi/2 <= teta <= 3pi/2 - tetaA
pRefTeta =r*((teta + tetaA +(pi/2) -cos(teta-tetaA))/(1 + sin(teta - tetaA)));
% Involute part sketching from tetaM to tetaA + pi/2
Xinv = r* sin(teta) - pInvTeta*cos(teta);
Yinv = -r*cos(teta)- pInvTeta*sin(teta);
invmin = 0;
invmax = tetaA + (pi/2);
% Reflector section sketching from tetaA + pi/2 to 3pi/2 - tetaA
Xref = r* sin(teta) - pRefTeta*cos(teta);
Yref = -r*cos(teta)- pRefTeta*sin(teta);
refmin = tetaA + (pi/2);
refmax = (3*pi)/2 - tetaA;
%plot
ezplot(Xinv,Yinv,[invmin,invmax]);
hold on
ezplot(Xref,Yref,[refmin,refmax]);
% reflect in x axis
ezplot(-Xinv,Yinv,[invmin,invmax]);
hold on
ezplot(-Xref,Yref,[refmin,refmax]);
% add absorber radius r centre at origin
x=0;
y=0;
ang=0:0.01:2*pi;
xp=r1*cos(ang);
yp=r1*sin(ang);
plot(x+xp,y+yp);
```

Appendix B: Data collection sheet

Date:_____

Time	T_1 (^oC)	T_2 (^oC)	ΔT (°C)	T_{amb} (^oC)	$I_{s,horizontal}$ (W/m^2)	$I_{s,Aperture}$ (W/m^2)